Mathematisches Forschungsinstitut Oberwolfach

Report No. 13/2020

DOI: 10.4171/OWR/2020/13

# Mechanics of Materials: Towards Predictive Methods for Kinetics in Plasticity, Fracture, and Damage

Organized by
Reinhold Kienzler, Bremen
David L. McDowell, Atlanta
Stefan Müller, Bonn
Ewald A. Werner, München

8 March – 14 March 2020

Abstract. The workshop dealt with current advances of computational methods, mathematics and continuum mechanics directed at thermodynamically consistent forms of constitutive equations for complex evolutionary phenomena in modern materials such as plasticity, fracture and damage. The main aspects addressed in presentations and discussions were multiphysical description of new materials, (visco)plasticity, fracture, damage, structural mechanics, mechanics of materials and dislocation dynamics.

*Mathematics Subject Classification (2010):* 74xx.

## Introduction by the Organizers

The workshop *Mechanics of Materials: Mechanics of Interfaces and Evolving Microstructure* attracted about 40 participants with broad geographic representation. Even though about 15 of the invited researchers canceled their participation shortly before the workshop due to the start of the SARS-CoV-2 pandemic, this workshop comprised a well balanced blend of researchers with backgrounds in mathematics, mechanics and materials science. The organizers successfully recruited a significant number of younger representatives of the mentioned research communities. The sequence and duration of the sessions were defined on Monday morning. They were moderated by session chairs and each consisted of 3-5 extended lectures (30 minutes each, including discussion) presented to all participants of the workshop. Ample time was devoted to discussion, both during and following presentations. The format of the sessions (subject to hard stops for lunch and dinner), including

coffee breaks, gave the flexibility to maximize productive discussion. Reports from the session chairs were summarized and discussed extensively on Friday and are summarized in this report.
The organizers regard this particular workshop as extremely successful in the topical area of mechanics of materials, for several reasons. First, a number of young participants were involved and highly active in presentations and discussions, representing the next generation of blending applied mathematics with mechanics of materials. Second, the discussions were detailed and deep into the subject, with many useful points and counterpoints discussed. We believe that this workshop has launched many potentially fruitful couplings of researchers, and has defined some specific target areas as goals for mathematics, mechanics and materials science.

One of the major advances of the past few decades has been the improvement of computational methods and applied mathematics directed at thermodynamically consistent forms of constitutive equations for complex non-equilibrium evolutionary phenomena such as plasticity, damage and fracture of materials. This includes methods for modelling material response at multiple spatial length scales. On the other hand, mathematical machinery and algorithms for addressing evolution of material structure occurring over a broad range of time scales is much less well developed. The fact that various structural attributes of materials (atoms, molecules, defects) have a spectrum of characteristic relaxation times is a key factor in limiting access to long time scales in modelling. It is a much more daunting problem, in general, than modelling spatial scale transitions alone. The conventional mathematical machinery of energy minimization provides guidance but has limited direct applicability to material systems evolving away from equilibrium. When microstructures evolve, as during plastic deformation, progressive damage and fracture, stress-assisted diffusion, migration or chemical/thermal aging, the associated classical mathematical frameworks are often ad hoc and heuristic. Advancing new and improved methods is a major focus of 21st century mechanics of materials. This state of affairs motivated the central theme of the workshop, namely to explore new and emerging mathematical approaches or schema to estimate and predict kinetics of fundamental processes in plasticity, damage and fracture. This requires a careful examination of various classes of modern constitutive theories for dislocation dynamics in metal plasticity ranging from coarse-grained atomistics to discrete dislocation dynamics and phase field models, for example, as well as defect cascades in fractures. Careful examination of transition state theory and entropic effects (both configurational and vibrational) is warranted. There are serious unresolved physical and mathematical issues and limitations in time up-scaling of predictive computational methods for up-scaling atomistic simulations to relevant time scales, and additional issues that pertain to modelling kinetics of evolution using continuum phase field models or discrete defect models. Based on the above sketch of current and highly relevant topics and the experience gained in organizing preceding workshops on mechanics of materials, five main topical working groups were suggested and the main results and numerous open questions of the dedicated sessions are summarized in the following sections.

## 1. Multiphysics

Multiphysical problems had received considerable attention on the theoretical side during the era of rational mechanics in the middle of the twentieth century. The field has continually gained fresh impetus since the 1990s from two main sources. Firstly, the emergence of new classes of materials that show strong multiphysical coupling effects (e.g. shape memory alloys and polymers, giant magnetostrictives, ferroelectrics, multiferroics, magneto- and electroactive polymers, etc.) – often classified as smart, active and/or multifunctional materials – has enabled new areas of technological application (smart actuators, sensors, and structures, energy harvesting, self-healing, data storage, biomimetics, substitute materials) that were previously simply inconceivable. Secondly, the rapid increase of computational power has led to the feasibility of incorporating complex constitutive behaviors, geometrical nonlinearity and multiscaling into the numerical treatment of multiphysics problems. However, despite decades of intense, multidisciplinary research efforts in the mathematical modeling of multiphysics systems, there remain many fundamental challenges, such as:

1) Even for many established continuum mechanics-based formulations capturing multifield coupling phenomena, fundamental mathematical analysis – e.g. proving the non-existence of solutions – is not available. This is particularly true, if nonlinearities, anisotropy and non-convexity come into play.

2) The calibration, verification, and validation of multiscale, multiphysics material models naturally proves particularly difficult. Since full sets of physical input parameters are almost never available from experimental measurements, the question arises on how uncertainties of various type – and statistical information in general – can be incorporated into multiphysical material models.

3) In addition to the lack of data, we now often face the difficulty of overdetermination, i.e. having too much data, possibly of very different origin or trustworthiness and containing undetected correlations. Data-driven materials science and machine-learning techniques, that currently receive enormous attention in many fields, may prove to be of particular merit in this regard.

4) In view of the ever increasing complexity of multiscale models, it is highly desirable to establish adaptive methods, for instance $FE^2$-techniques for structural computation, in which direct numerical homogenization from the lower length-scale is activated only if triggered by an appropriate error estimator.

5) New classes of concurrent multiscale methods centering on reduced-order modeling (e.g. proper generalized decomposition) are beginning to emerge, along with the data-driven methods (e.g. self-consistent clustering analysis) to complement the $FE^2$ approach. Much work will be needed to investigate the full potential – and limitations – of these methods.

6) Finally, all of the developments discussed in the other working groups also bear great relevance to multi-physics problems. In our experience, much fundamental understanding and also novel theoretical and numerical techniques that were originally developed in the multiphysics context can vice versa lead to new approaches in more classical research areas.

## 2. (Visco)Plasticity

Important and stimulating talks and discussions centered around the following topics.
1) Smooth rate-independent elastoplastic models are physically more realistic than standard ones with a kink at yield. They are also computationally advantageous due to the absence of consistency condition to be exploited. Implications of strain localization analysis have been investigated recently.
2) Invariance principles in mechanics are instrumental in the derivation reduced forms of constitutive equations. The methodology has been recently applied to second gradient fluids. Applications to turbulence have been highlighted and to blood flow in vessels. Such models are mature for CFD.
3) Quite current is the mathematical modelling of energetic materials that have large amounts of stored chemical energy. It is then imperative to describe simultaneously the mechanics and the thermodynamics of the body. The presented model attempts to describe an archetypal thermo-mechanical phenomenon: shear banding. It is challenging to analyse the equations for heat flow within thermo-mechanical bodies when their material parameters are temperature-dependent. There is a need for a rigorous mathematical treatment of internal energy in different material types, for the existence theory for the parabolic free boundary problem that arises in the shear band model, as well as a call for empirical data from experiments.
4) Crystal plasticity models involve sophisticated constitutive equations accounting for the kinetics of dislocation multiplication and storage depending on stress and strain rate. Parameter identification from macroscopic tensile tests over a large range of temperatures turns out to be a challenging issue. A discussion followed on the most suitable form for the viscoplastic slip rate function with proposals from the audience. Suggestions followed regarding the use of strain rate jump tests and relaxation tests.
5) A hierarchy of viscoplasticity models emerges from the discussion: from the most simple $J_2$ plasticity model to crystal plasticity and strain gradient models. They are ready for goal-oriented model adaptative schemes.

## 3. Fracture, damage and structural mechanics

The most important outcomes of the talks and discussions are as follows.
1) In the field of fracture and damage models as rate-independent systems it became clear, that different approaches lead to different solutions. So far, it is not evident, which approach can be considered as the correct one.
2) Cavitation is a process, that is known in fluid dynamics for a long time. The occurrence in solid mechanics and its interpretation as fracture is a quite new development. Of special interest seems to be the occurrence of hardening (in coexistence with strain-induced crystallization) and healing, thus introducing a negative rate of damage.
3) It became obvious, that the mathematical research concerning the development of cracks might improve the computation of damage of fiber reinforced materials

using phase-field approaches. The use and determination of appropriate material properties of heterogeneous materials taking into account the actual microstructure is a central aspect to obtain reliable results. The simulation of fatigue of materials with plastic deformation can be done in a timely more efficient way as it has been presented, but for larger plastic zones, a more detailed computation of the plastic zones might be necessary.
4) Findings are related to new areas for the use of metamaterials such as pantographic structures, large elastic deformations, high-damage tolerances, deployable structures or simply engineered material with special properties, discrete models for higher-order gradient materials.
5) An a priori error estimate for consistent plate theories is difficult and important, especially when results need to be reliable. This includes boundary conditions. The discussion showed the necessity to put more effort into the differentiability of the used approximations for the description of e.g. the loading. Localization of errors, not only for stress resultants but also for stresses should be taken into account. Oscillations of stresses at corners should be investigated as well.

## 4. Mechanics of materials

The session was devoted to the field of mechanics of materials itself. It comprised a wide mixture of topics ranging from mathematical aspects to engineering applications.
1) The mathematically oriented contributions demonstrate that the impact of mathematics to the field are of utmost importance since rigorous checks and proofs of suggested models of the material behavior are necessary for applications, especially if computer simulations should be realized.
2) Several application oriented contributions have shown the diversity of research in the field of mechanics of materials. Solving practical problems in the case of advanced materials, improvement of materials properties, data handling, and new applications are only a few examples.
3) The interpretation of the term mechanics of materials is not unique as it ranges from the classical term strength of materials up to the German term Werkstoffmechanik. The last one is more general, since it aims to abstract the material behavior by equations taking into account the kinetics of microstructure evolution due to processing and/or service conditions.

## 5. Dislocations

With regard to the continuum dislocation dynamics CDD theories, the constitutive closure for the average dislocation velocity was discussed as a persistent challenge which deserves special attention and possibly the development of novel approaches. Classical continuum thermodynamics as well as the GENERIC framework show weaknesses when applied to dislocation systems. The reason is on the one hand the complexity of the developing dislocation networks, and on the other hand, that dislocations are mostly in metastable states without being much affected by thermal activation at low homologous temperatures. With regard to the universal

laws the discussions addressed the question of the predictive power of the presented theories.
1) One talk explained how CDD defines a crystal plasticity theory solely built upon transport or transport-reaction equations for vectorial or tensorial dislocation density measures. Constitutive modelling in CDD based crystal plasticity therefore means the provision of a relation between the current stress and dislocation state and the average dislocation velocity, rather than a stress-shear-rate relation, which defines phenomenological crystal plasticity. Focus was put on the incorporation of dislocation reactions and cross-slip in the CDD framework, in order to capture well-known processes on the single dislocation level within the continuum framework. It was demonstrated that according large-scale CDD simulations reproduce salient features of strain hardening in single crystals and dislocation pattern formation, both in uni-directional and in cyclic loading. Furthermore it was shown how averaged CDD theories may be developed which overcome restrictions on the spatial resolution, which are present in dislocation density-vector based CDD theories. Finally, it was concluded that large deformation CDD needs to be coupled to evolving fields of point defects, most notably vacancies.
2) The General Equation for Non-Equilibrium Reversible Irreversible Coupling (GENERIC) is a tool for deriving the above mentioned closure, i.e., deriving the average dislocation velocity in CDD formulations as a function of the current stress and dislocation state. The presented approach was based on the general elastic interaction energy functional for curved dislocation networks from dislocation field theory. In particular, this formulation results in coarse-grained continuum balance, transport, and thermodynamic flux-force, relations depending on the underlying discrete energetics and dynamics.
3) A further talk introduced a polycrystal theory based on evolution laws for scalar dislocation densities. Focus was laid on capturing the strain-rate and temperature dependence of polycrystalline metals in the spirit of constitutive laws based on thermally activated dislocation motion as first introduced by U.F. Kocks. However, the presented work heavily built on recent work by J.S. Langer, where the usual exponential Arrhenius law for the strain rate, with power law dependencies on the stress in the exponential, is replaced by a double exponential dependency on the stress.

*Acknowledgement:* The MFO and the workshop organizers would like to thank the National Science Foundation for supporting the participation of junior researchers in the workshop by the grant DMS-1641185, "US Junior Oberwolfach Fellows".

## Workshop: Mechanics of Materials: Towards Predictive Methods for Kinetics in Plasticity, Fracture, and Damage

### Table of Contents

# Abstracts

## Electric Power Absorption Caused Thermal Tissue Damage

Bilen Emek Abali

Electrically induced tissue damage is a coupled phenomenon in multiphysics. Conducting electricity produces heat and this increases the temperature. The soft tissue – skin, organs, brain, or muscles – is burnt under successive heating. This thermal damage is modeled by using a scalar field called a damage parameter with a corresponding evolution law. Electromagnetism, thermomechanics, and damage modeling creates a set of coupled and nonlinear field equations. The correct weak formulation is challenging in the case of a numerical implementation with the aid of the finite element method. The reasons of this difficulty is discussed and a possible remedy is shown allowing a monolithic as well as robust computational implementation of the electromagneto-thermomechanics damage simulation.

### 1. Interaction of Electromagnetism and Thermomechanics

Mechanical and electric energy are transferable such that there is a strong coupling between these fields. Consider the balance of mechanical momentum in a "material" frame for obtaining displacement, $\boldsymbol{u}$, depending on the momentum flux or usually called engineering stress,[1] $\boldsymbol{P}$, as follows:

$$\rho_0 u_i^{\bullet\bullet} - P_{ji,j} - \rho f_i = \mathcal{F}_i \ , \tag{1}$$

where the mass density, $\rho_0$, is a given function in space, $\boldsymbol{X}$, gravitational (specific, i.e. per mass) body force, $\boldsymbol{f}$, is often modeled as a constant. Einstein's summation convention is understood for repeated indices. A comma denotes a space derivative, all fields are expressed in Cartesian coordinates. The coupling term, $\boldsymbol{\mathcal{F}}$, is the ponderomotive force density, in the case of non-polarized material,

$$\mathcal{F}_i = \rho z \mathcal{E}_i + \epsilon_{ijk} \mathcal{J}_j B_k \tag{2}$$

is called the Lorentz force with the electric field, $\boldsymbol{\mathcal{E}}$, and magnetic flux, $\boldsymbol{\mathcal{B}}$, measured on the "material" frame. In the case of polarized material, the discussion is tedious and a definition seems to be arduous, known as the Abraham–Minkowski controversy, see for example [1, 2, 3, 4, 5]. Already in the Lorentz force, we realize that the mass density, $\rho$, and specific charge, $z$, are given with respect to material (meaning mass) positions at the current placement, although the formulation for mechanics is in the material frame often chosen as the initial placement. The transformation between them is well known for thermomechanical fields, where coordinate transformation is used for fields leading to a Euclid transformation. The same transformation fails to hold for electromagnetic fields and the Maxwell equations. The coupling is of interest, but it seems to be very

[1] Stress on a material frame is called the Piola or Boussinesq or first Piola–Kirchhoff stress

difficult to develop a unique theory. By starting from FARADAY's law, we obtain two MAXWELL equations with the following ansatz functions fulfilling them

$$E_i = -\phi_{,i} - \frac{\partial A_i}{\partial t} \ , \quad B_i = \epsilon_{ijk} A_{k,j} \ , \tag{3}$$

electric field, $\boldsymbol{E}$, magnetic flux (area density), $\boldsymbol{B}$, are given by electric potential, $\phi$, magnetic potential, $\boldsymbol{A}$. All fields are measured on a laboratory frame assumed to be fixed in space. This solution is adequate, but $\boldsymbol{E}$ and $\boldsymbol{B}$ consist of 6 components and cannot be described uniquely by $\phi$ and $\boldsymbol{A}$ related 4 components. The missing conditions are called "gauge" conditions and we can freely choose rate of electric potential and divergence of magnetic potential. Electromagnetic fields, $\boldsymbol{E}$, $\boldsymbol{B}$, will remain the same. They are the real measurable quantities and their transformation properties are given by

$$\mathcal{E}_i = E_i + \epsilon_{ijk} u_j^{\cdot} B_k \ , \quad \mathcal{B}_i = B_i \ , \tag{4}$$

as well as $J_i = \mathcal{J}_i + \rho z u_i^{\cdot}$. Obviously, the transformation is different between two frames, we ignore the difference and use "space" in a lax terminology as being the reference frame equal to the material frame for thermomechanics and electromagnetism. As a gauge condition, one is free to choose any combination, for computational performance, we choose the LORENZ gauge condition:

$$\frac{\partial \phi}{\partial t} = -\frac{1}{\mu_0 \varepsilon_0} A_{i,i} \ , \tag{5}$$

with the universal constants, $\varepsilon_0$, $\mu_0$, and we refer to [6] for computational implementations. From the balance of charge, we obtain another two MAXWELL equations

$$\frac{\partial \rho z}{\partial t} + J_{i,i} = 0 \ , \quad \rho z = D_{i,i} \ , \quad \frac{\partial D_j}{\partial t} = \epsilon_{jkl} H_{l,k} - J_j \ . \tag{6}$$

with MAXWELL–LORENTZ aether relations:

$$D_i = \varepsilon_0 E_i \ , \quad H_i = \frac{1}{\mu_0} B_i \ . \tag{7}$$

By using the latter, field equations for $\phi$, $\boldsymbol{A}$ read

$$\frac{\partial D_{i,i}}{\partial t} + J_{i,i} = 0 \ , \quad \varepsilon_0 \frac{\partial^2 A_i}{\partial t^2} - \frac{1}{\mu_0} A_{i,kk} - J_i = 0 \ , \tag{8}$$

respectively. For the balance of internal energy, supply term, $r$ is known, stress, $P_{ji} = F_{ik} S_{jk}$, is given by the material stress, $\boldsymbol{S}$, with the deformation gradient, $F_{ij} = u_{i,j} + \delta_{ij}$, as follows:[2]

$$\rho_0 u^{\cdot} + Q_{i,i} - \rho_0 r = J \mathcal{J}_i \mathcal{E}_i + S_{ij} \varepsilon_{ij}^{\cdot} \ , \quad J = \det(\boldsymbol{F}) \ , \tag{9}$$

where the heat flux, $\boldsymbol{Q}$, needs to be modeled, the specific internal energy, $u$, is modeled by the specific HELMHOLTZ heat energy, $f = u - T\eta$. Temperature, $T$,

[2]Rate denoted by dot is an objective time derivative tantamount to the partial time derivative in the material frame.

is the unknown and specific entropy, $\eta$, needs to be defined. If we use a FUNG material model:

$$u = c(T - T_{\mathrm{Ref}}) + \frac{D}{\rho_0}\left( \exp\left(\frac{1}{2}\varepsilon_{ij} B_{ijkl} \varepsilon_{kl}\right) - 1\right) , \tag{10}$$

with the damage variable, $\alpha$, we observe that $f = f(T, \boldsymbol{\varepsilon}, \alpha)$. Relations,

$$\eta = \frac{\partial f}{\partial T} , \quad S_{ij} = \rho_0 \frac{\partial f}{\partial \varepsilon_{ij}} = C_{ijkl}\varepsilon_{kl} , \tag{11}$$

allow us to obtain the balance of internal entropy:

$$\rho_0 \eta^{\cdot} + \left(\frac{Q}{T}\right)_{,i} - \rho_0 \frac{r}{T} = \Sigma , \quad \Sigma = -\frac{Q_i}{T^2} T_{,i} + \frac{J}{T} \mathcal{J}_i \mathcal{E}_i - \frac{\rho_0}{T}\frac{\partial f}{\partial \alpha}\alpha^{\cdot} . \tag{12}$$

According to the second law of thermodynamics, $\Sigma \geq 0$, we obtain the following conclusion according to the CURIE principle,

$$-\frac{\rho_0}{T}\frac{\partial f}{\partial \alpha}\alpha^{\cdot} \geq 0 , \quad \frac{\varepsilon_{ij} C^0_{ijkl} \varepsilon_{kl}}{2T\alpha^2} \exp\left(\frac{1}{2D\alpha} \varepsilon_{mn} C^0_{mnop} \varepsilon_{op}\right)\alpha^{\cdot} \geq 0 , \tag{13}$$

such that $\alpha^{\cdot} \geq 0$, analogous to the KARUSH–KUHN–TUCKER condition. A simple model relies on a positive rate activated beyond a threshold value. Now for the other terms, we utilize, for the sake of simplicity, linear relations,

$$Q_i = -\kappa T_{,i} + \varsigma \pi T \mathcal{E}_i , \quad \mathcal{J}_i = \varsigma \pi T_{,i} + \varsigma \mathcal{E}_i . \tag{14}$$

## 2. Weak formulation

We discretize in time by using the finite difference method, $\partial()/\partial t = \big(() - ()^0\big)/\Delta t$, with the known (computed) solution $()^0$ at the last time step. In space, we use the finite element method and obtain the weak form by multiplying by test functions, performing integration by parts, as well as apply jump conditions—especially for electromagnetic potentials, jump conditions are crucial, we refer to [7] for a verification of the numerical procedure by an analytical solution. We emphasize that the total weak form is the sum of all weak forms for each unknown, namely,

$$\text{Weak Form} = \mathrm{F}_{\phi} + \mathrm{F}_{\boldsymbol{A}} + \mathrm{F}_{\boldsymbol{u}} + \mathrm{F}_T . \tag{15}$$

Hence, each weak form has to be in the same unit. All unknowns are from the same space

$$\mathcal{V} = \left\{ \{\phi, A_1, A_2, A_3, u_1, u_2, u_3, T\} \in [\mathcal{H}^1(\Omega)]^8 : \{\phi, A_i, u_i, T\}\Big|_{\partial\Omega} = \text{given} \right\} . \tag{16}$$

This choice is possible as we have chosen the LORENZ gauge. In this case, electromagnetic potentials generate the following weak forms:

$$\begin{aligned} \mathrm{F}_{\phi} &= \sum_{\text{ele}} \int_{\Omega} \Big( -(D_i - D_i^0)\delta\phi_{,i} - \Delta t J_i \delta\phi_{,i} \Big)\, \mathrm{d}V , \\ \mathrm{F}_{\boldsymbol{A}} &= \sum_{\text{ele}} \int_{\Omega} \left( \varepsilon_0 \frac{A_i - 2A_i^0 + A_i^{00}}{\Delta t^2}\delta A_i + \frac{1}{\mu_0} A_{i,j}\delta A_{i,j} - J_i \delta A_i \right) \mathrm{d}V . \end{aligned} \tag{17}$$

The computational domain, $\Omega$, is simply the triangulation of the physical domain and the boundary conditions as well as jump conditions are of importance, we direct to [8] for further details as well as convergence analysis. For thermomechanical fields we have

$$\mathrm{F}_{\boldsymbol{u}} = \sum_{\mathrm{ele}} \int_{\Omega} \left( \rho_0 \frac{u_i - 2u_i^0 + u_i^{00}}{\Delta t^2} \delta u_i + P_{ji} \delta u_{i,j} - \rho f_i \delta u_i - \mathcal{F}_i \delta u_i \right) \mathrm{d}V \ ,$$

$$\mathrm{F}_T = \sum_{\mathrm{ele}} \int_{\Omega} \left( \rho_0 (\eta - \eta^0) \delta T - \Delta t \frac{Q_i}{T} \delta T_{,i} - \Delta t \rho_0 \frac{r}{T} \delta T - \Delta t \Sigma \delta T \right) \mathrm{d}V + \int_{\partial\Omega} \frac{\Delta t}{T} h (T - T_{\mathrm{amb}}) \delta T \, \mathrm{d}A \ , \tag{18}$$

where for temperature, we use so-called natural boundary conditions with the convection parameter, $h$. The damage parameter is updated as

$$\alpha := \alpha + \Delta t \dot{\alpha} \ , \tag{19}$$

where ":=" denotes an assigning new values operator in computational algebra. Weak formulation for a multiphysics application including displacement, temperature, electromagnetism, as well as thermal damage has been briefly shown. We emphasize that this weak form is delivering a robust method to simulate applications even under loading leading to high rates of unknowns as demonstrated in [8].

## References


[1] Y. N. Obukhov, *Electromagnetic energy and momentum in moving media*, Annalen der Physik **17**(9-10) (2008), 830–851.

[2] M. Mansuripur, *Resolution of the Abraham–Minkowski controversy*, Optics Communications **283**(10) (2010), 1997–2005.

[3] D. J. Griffiths, *Resource letter EM-1: Electromagnetic momentum*, American Journal of Physics **80**(1) (2012), 7–18.

[4] M. Bethune-Waddell, K. J. Chau, *Simulations of radiation pressure experiments narrow down the energy and momentum of light in matter*, Reports on Progress in Physics **78**(12) (2015), 122401.

[5] B. E. Abali, A. F. Queiruga, *Theory and computation of electromagnetic fields and thermomechanical structure interaction for systems undergoing large deformations*. Journal of Computational Physics **394** (2019), 200–231.

[6] B. E. Abali, *Computational Reality, Solving Nonlinear and Coupled Problems in Continuum Mechanics*, Advanced Structured Materials vol. 55., Springer Nature, Singapore 2017.

[7] B. E. Abali, F. A. Reich. *Verification of deforming polarized structure computation by using a closed-form solution*, Continuum Mechanics and Thermodynamics **30** (2018), 1–16.

[8] B. E. Abali,T. I. Zohdi, *Multiphysics computation of thermal tissue damage as a consequence of electric power absorption*, Computational Mechanics **65** (2020), 149–158.

## Mechanics of Materials - Werkstoffmechanik

Holm Altenbach

The material life cycle comprises different stages (Fig. 1). It is easy to see that some of these stages belong to Mechanics of Materials. But at first one should clarify the meaning of Mechanics of Materials.
From the internet one gets the following information concerning Mechanics of Materials:

- Mechanics of Materials is an international journal (founding editor S. Nemat-Nasser, Elsevier).
- Wikipedia [2]: **Strength of materials**, also called **mechanics of materials**, deals with the behavior of solid objects subject to stresses and strains. The complete theory began with the consideration of the behavior of one and two dimensional members of structures, whose states of stress can be approximated as two dimensional, and was then generalized to three dimensions to develop a more complete theory of the elastic and plastic behavior of materials. An important founding pioneer in mechanics of materials was **Stephen Timoshenko**.
- Translation: **Mechanics of Materials** $\leftrightarrow$ **Werkstoffmechanik** [3].

Mechanics of Materials is an interdisciplinary topic in between Materials Science, (Continuum) Mechanics, (Applied) Mathematics. The focus is on the description of the material behaviour by equations. The outcome is computer simulation of

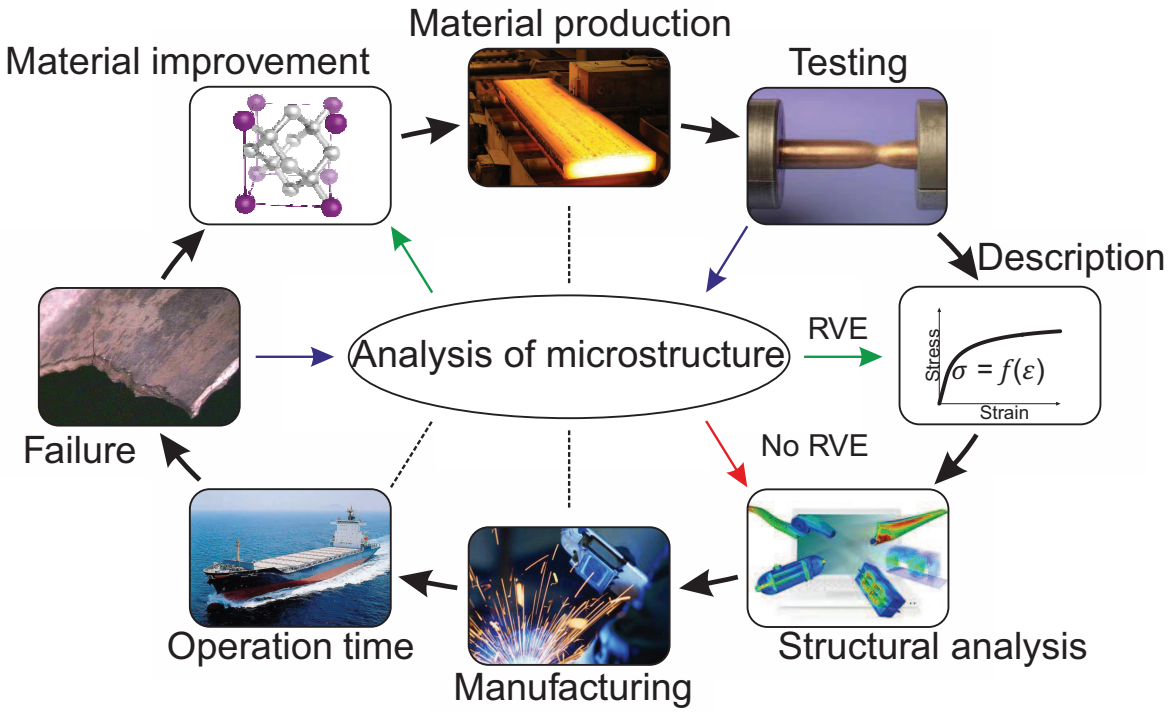


Figure 1. Material life cycle [1]

tests with simple specimens an of structural elements or structures. There are the following challenges

- Identification of the material parameters or parameter functions,
- Verification of the models,
- Mathematical correctness of the models, and
- Physical admissibility of the models.

One direction of Mechanics of Materials is related to the basic equations of Continuum Mechanics [4]. For solving problems we need:

- first set of equations
  - kinematical relations,
  - statements w.r.t. loadings,
  - balance equations
    - mass,
    - momentum,
    - moment of momentum,
    - energy,
    - entropy,
- second set of equations
  - constitutive and
  - evolution equations.

In addition, one needs

- boundary and/or initial conditions
- jump conditions, if the physical fields are non-smooth.

There are several extensions to the classical statements discussed during this conference, e.g. **Gradient Theories**, **Cosserat theories** or **Multiphysics**.
The second set of equation are the material-dependent equations. They are specific for each material since they are describing the individual response of the continuum on loading (mechanical, thermal, electrical,magnetic, etc.). Constitutive equations can be algebraic (e.g. Hooke's law), differential (e.g. creep law), integral (viscoelatic behaviour), etc. Evolution equations are differential equation of first order w.r.t. time describing evolution processes like damage in the material.
Mechanics of Materials is also focused on scales. The classical scales are: the macroscopic scale (phenomenological description of the material behavior on the base of experimental observations and a mathematical framework), microscopic scale (description of the microstructural changes, for example, texture, damage, phase transitions, etc.), and the atomistic scale (description of the interatomic actions, for example, by assuming force potentials). Now, we have also other (more) scales, for example, the mesoscale (between macro- and microscale) or the submicroscale.
The constitutive behavior can be modeled on the base of Materials Physics, Materials Science, and Mechanics. Material physics is the use of physics to describe materials. It is a synthesis of physical sciences such as chemistry, solid mechanics and solid state physics. Solid-state physics is the largest branch of condensed

matter physics, is the study of rigid matter, or solids. The bulk of solid-state physics theory and research is focused on crystals, largely because the periodicity of atoms in a crystal – its defining characteristic – facilitates mathematical modeling, and also because crystalline materials often have electrical, magnetic, optical, or mechanical properties that can be exploited for engineering purposes. Materials science or materials engineering is an interdisciplinary field involving the properties of matter and its applications to various areas of science and engineering. This science investigates the relationship between the structure of materials and their properties. It includes elements of applied physics and chemistry, as well as mechanical, civil and electrical engineering.
In Mechanics we have three modeling approaches. The first is the **Top-down Modeling** (deductive approach). The starting point of the deductive approach is the introduction of axioms of the material theory: causality, determinism, equipresence, material objectivity, local action, memory, and physical consistency, etc. The second approach **Bottom-up Modeling** (inductive approach) is a more engineering way of formulation constitutive equations. For example, we start we the Hooke's law (tension with $\sigma$ - normal stress, $E$ - Young's modulus and $\varepsilon$ normal strain

$$\sigma = E\varepsilon$$

or torsion with $\tau$ - shear stress, $G$ - shear modulus and $\gamma$ - shear strain

$$\tau = G\gamma$$

and generalize towards the following cases: three-dimensional isotropic case, three-dimensional anisotropic case, nonlinear behavior, .... In each case, the thermodynamical consistency, which is guaranteed in the deductive approach, should be checked separately. The last approach is the **Rheological Modeling**. This approach is founded on the introduction of some basic models, for example, related to elastic behavior, plastic behavior, and viscous behavior. In addition, the assumption that the connection of basic models can be realized only in parallel or series. Then any complex behavior can be represented by these connection, for example, visco-elastic = elastic + viscous or visco-plastic = plastic + viscous. Important contributions to the last one field were made Markus Reiner (1886-1976) and discussed, for example, by Arnold Krawietz and Vladimir Palmov (1934-2018). The last one realized this approach in the case of isotropic and anisotropic materials including large strains.

## References

[1] O. Prygorniev, *Statistical analysis of stress and deformation state in polycrystalline aggregates with a large number of grains*, PhD Thesis, University of Magdeburg, 2015.
[2] https://en.wikipedia.org/wiki/Strength_of_materials (12.03.2020).
[3] https://context.reverso.net/Übersetzung/deutsch-englisch/Werkstoffmechanik.
[4] H. Altenbach, *Kontinuumsmechanik - Einführung in die materialunabhängigen und materialabhängigen Gleichungen*, 4th ed., Springer Vieweg, 2018.

## On Invariance Requirements for Gradient Fluids

Albrecht Bertram

In 1867 Levy [1] and de Saint-Venant [2] stated that the measured velocity profiles of turbulent channel flows can not be simulated neither by a (linear) Navier-Stokes law nor by a non-linear extension of it. On this occasion, de Saint-Venant already suggested to take higher velocity gradients into account.
A century later Trostel made the same suggestion. His intention was to describe fully developed turbulence, and he and his group worked out a theory of second-order [3] and third-order linear fluids [4]. For such models, invariance requirements play a crucial role, and are not always correctly stated. Three main issues are involved

1. invariance under change of observer (objectivity)
2. invariance under superimposed rigid body modifications
3. invariance under symmetry transformations

These three invariances must be carefully distinguished.
The first one leads to the objectivity of the stress tensors, and should hold for all materials.
The second allows for reduced forms of the stress laws. In fact, a necessary and sufficient condition for this invariance to hold is that the stress laws are hemitropic functions of the kinematical ones [5, 6]. However, it may be questioned if or how far this invariance can be assumed for turbulent flows.
In contrast to the first and second invariance requirement, the third one is less controversial. One usually defines a fluid by its symmetry group as being formed by the whole unimodular group. One has to keep in mind that a symmetry transformation is usually introduced as a change of the reference placements which lets the material law unaltered [7]. In the case of viscous and incompressible fluids the description can be made fully Eulerian so that no reference placement is involved. In such a case the symmetry group is automatically the maximal one, i.e., the proper unimodular group.
If we restrict our concern to second order linear viscous fluids, one can start with a dissipation potential as a square form in the first and second velocity gradients. Such square forms are given by material tensors of fourth, fifth, and sixth order. Lists of hemitropic tensors of these orders can be found in [8, 9, 10, 11], and others. The complete dissipation potential, the resulting stress laws, and the equation of motion for such materials are given by [5, 6].
Because of the assumed incompressibility of our fluid, we have the classical internal constraint $\operatorname{div} \boldsymbol{v} = 0$ and the non-classical one $\operatorname{grad} \operatorname{div} \boldsymbol{v} = 0$. Consequently, some of the terms in the dissipation potential vanish. On the other hand, reaction stresses have to be added, see [14]. One is a spherical part in the second-order stress tensor standing for the usual hydrostatic pressure. But additionally, three third-order hyperstresses appear, so that finally four scalar fields of the reactive parts are present in the balance equation for the linear momentum. This has not been considered by Trostel [3] and Silber [4].

Applications to turbulence can be found in [13] and to blood flow in [12].

## References


[1] M. Levy, *Essai théorique et appliqué sur le mouvement des liquides*, Ponts et Chaussées, Thesis, 1867.

[2] A. J. C. B. de St.-Venant, *Rapport sur un mémoire de M. Maurice Levy, relatif à l'hydromechanique des liquides homogènes, particulièrment à leur écoulement rectiligne et permantent*, C R Acad. Sci. Paris **68** (1869), 582–592.

[3] R. Trostel, *Gedanken zur Konstruktion mechanischer Theorien.* In: *Beiträge zu den Ingenieurwissenschaften*, R. Trostel (Ed.), Univ.-Bibl. Techn. Univ. Berlin (1985), 96–13.

[4] G. Silber, *Eine Systematik nichtlokaler kelvinhafter Fluide vom Grade drei auf der Basis eines klassischen Kontinuumsmodelles*, Fortschritt-Berichte VDI Nr. 26 (1986).

[5] A. Bertram, *On viscous gradient fluids*, Continuum Mech. Thermdyn. (2019), DOI:10.1007/s00161-019-00853-4.

[6] A. Bertram, Compendium on Gradient Materials, https://www.lkm.tu-berlin.de/fileadmin/fg49/publikationen/bertram/Compendium_on_Gradient_Materials_June_2019.pdf (2019).

[7] C. A. Truesdell, W. Noll, *The Non-linear Field Theories of Mechanics*, In: *Handbuch der Physik*. Vol. III/3. S. Flügge (ed.), Springer, Berlin 1965.

[8] U. Cisotti, *Tensori quintupli emisotropi*, Rend. d. Reale Acad. Naz. dei Lincei **12**(2) (1932), 195–199.

[9] B. Caldonazzo, *Osservazione sui tensori quintupli emisotropi*, Rend. d. Reale Acad. Naz. dei Lincei **15** (1932), 840–843.

[10] H. Weyl, *The classical groups: their invariants and representations*, Princeton University Press, 1939.

[11] E. A. Kearsley, J. T. Fong, *Linearly independent sets of isotropic Cartesian tensors of ranks up to eigtht*, J. Research Nat. Bur. Stand. B. Mathematical Sciences **79B**(1-2) (1975).

[12] G. Silber, *Gradiententheorien in der biomedizinischen Physik*, In: *Beiträge zur Mechanik*, Trostel-Festschrift, C. Alexandru, G. Gödert, U. Görn, R. Parchem, J. Villwock (Eds) (1993), 308–324.

[13] G. Silber, M. Alizadeh, *Zylinderspaltströmungen von Fluiden vom Grade zwei bei realen Randbedingungen*, Mechanik - Gummert Festschrift, P. Oberweis (Ed). Techn. Univ. Berlin (1998), 187–202.

[14] A. Bertram, R. Glüge, *Gradient Materials with Internal Constraints*, Mathematics and Mechanics of Complex Systems **4**(1) (2016), 1–15, DOI: 10.2140/memocs.2016.4.1.


## On smooth rate–independent isotropic and crystal plasticity


Samuel Forest

(joint work with Miles B. Rubin)


### 1. Smooth rate–independent isotropic elastoplasticity

The smooth rate-independent elastoplasticity model discussed here was pointed out by M. B. Rubin recently [1, 2]. It introduces a rate–independent overstress whose influence on plastic failure modes has been studied recently [3, 4].

Smooth and standard $J_2$ rate–independent isotropic elastoplasticity share the following common features, here presented within the small strain framework for brevity:

- Elastic strain tensor, $\boldsymbol{\varepsilon}_e$
- Deviatoric strain and elastic strain tensors, $\boldsymbol{\varepsilon}', \boldsymbol{\varepsilon}'_e \quad \boldsymbol{\varepsilon}' = \boldsymbol{\varepsilon} - \frac{1}{3}(\boldsymbol{\varepsilon} : \mathbf{1})\mathbf{1}$
- Equivalent elastic strain measure $\gamma_e = \sqrt{\frac{2}{3}\boldsymbol{\varepsilon}'_e : \boldsymbol{\varepsilon}'_e}$
- Yield function
$$g(\gamma_e, \kappa) = 1 - \frac{\kappa}{\gamma_e}$$
- Evolution law for elastic strain $\dot{\boldsymbol{\varepsilon}}_e = \dot{\boldsymbol{\varepsilon}} - \Gamma \boldsymbol{\varepsilon}'_e$
- Evolution of the hardening variable
$$\dot{\kappa} = m(\kappa_s - \kappa)\Gamma = H\Gamma\gamma_e, \quad \kappa(0) = \kappa_0$$
- Stress and plastic strain based presentation
$$f(\boldsymbol{\sigma}, \kappa) = J_2(\boldsymbol{\sigma}) - 2\mu\kappa, \quad J_2(\boldsymbol{\sigma}) = \sqrt{\frac{3}{2}\boldsymbol{\sigma}' : \boldsymbol{\sigma}'} = 2\mu\gamma_e$$
$$\dot{\boldsymbol{\varepsilon}}^p = \dot{p}\frac{3}{2}\frac{\boldsymbol{\sigma}'}{J_2(\boldsymbol{\sigma})} = \Gamma\boldsymbol{\varepsilon}'_e, \quad \Gamma = \frac{3}{2}\frac{\dot{p}}{\gamma_e}$$
- Equivalent deviatoric strain rate measure $\dot{\varepsilon} = \sqrt{\frac{2}{3}\dot{\boldsymbol{\varepsilon}}' : \dot{\boldsymbol{\varepsilon}}'}$

The difference lies in the definition of the intensity of plastic flow as
$$\Gamma = b < g(\gamma_e, \kappa) > \dot{\varepsilon}$$
which is a homogeneous function of degree 1 leading to rate–independence. It involves a new parameter $b$ characterizing the overstress. This is in contrast to the standard model
$$g = 0, \quad \dot{g} = 0 \quad \Longrightarrow \quad \Gamma = \frac{3}{2\gamma_e^2}\frac{< \boldsymbol{\varepsilon}'_e : \dot{\boldsymbol{\varepsilon}} >}{1 + H}$$
for which the plastic multiplier is obtained from the consistency condition.
The properties of the smooth rate–independent overstress model are the following

- The model is rate–independent
$$\dot{\boldsymbol{\varepsilon}}_e = \dot{\boldsymbol{\varepsilon}} - b < g > \dot{\varepsilon}\, \boldsymbol{\varepsilon}'_e$$
- The model is smooth at yield;
- There exists an overstress and there is no consistency condition;
- The model tends to the standard one for $b \to \infty$
- The tangent elastoplastic operator is not symmetric which has consequences on strain localization properties [4].

## 2. Smooth rate–independent crystal plasticity

The previous smooth approach to elastoplasticity can be extended to anisotropic media like single crystals. The method is in fact particularly effective in that case because it gives a solution to a long–standing problem in quasi–rate–independent crystal plasticity. Standard rate–independent crystal plasticity models namely suffer from the indeterminacy problem of activated slip systems if the number of available slip systems is too large, as it is the case in FCC crystals [5]. Various remedies are available currently:

- Viscoplastic regularization: A viscous overstress is introduced which should remain small enough in the studied range of strain rates [6];
- Selection based on maximal plastic dissipation [7, 8];
- Unified power-law yield function [9, 10, 15];
- Pseudo-inverse used as an active set selection method [12, 13];
- Algorithmic active set selection [11, 14];
- The smooth rate–independent crystal plasticity model proposed in [16].

The modification of the classical crystal plasticity framework is minimal as it is now explained. The usual Mandel multiplicative decomposition is used

$$\boldsymbol{F} = \boldsymbol{E}\boldsymbol{P}$$

Crystallographic plastic flow results from the contribution of $N$ slip systems:

$$\dot{\boldsymbol{P}}\boldsymbol{P}^{-1} = \sum_{s=1}^{N} \dot{\gamma}^s \, \boldsymbol{\ell}^s \otimes \boldsymbol{n}^s$$

where $\dot{\gamma}^s$ is the individual slip rate for slip system $s$ defined by the slip direction $\boldsymbol{\ell}^s$ and the normal to the slip plane $\boldsymbol{n}^s$. The resolved shear stress is computed from the Mandel stress tensor:

$$\tau^s = \boldsymbol{M} \cdot (\boldsymbol{\ell}^s \otimes \boldsymbol{n}^s), \quad \text{with} \quad \boldsymbol{M} = (\det \boldsymbol{E})\, \boldsymbol{E}^T \boldsymbol{\sigma} \boldsymbol{E}^{-T}$$

We introduce again an equivalent total distortional strain rate

$$\dot{\varepsilon} = \sqrt{\frac{2}{3}\boldsymbol{D}' \cdot \boldsymbol{D}'}$$

The Schmid law is still of the form

$$f^s(\boldsymbol{\sigma}, x^s, r^s) = |\tau^s - x^s| - r^s$$

The modification of the standard model consists in replacing the usual viscoplastic flow rule by the rate–independent one:

$$\dot{\gamma}^s = \left\langle \frac{f^s}{K} \right\rangle^n \operatorname{sign}(\tau^s - x^s) \quad \Longrightarrow \quad \dot{\gamma}^s = \dot{\varepsilon} \left\langle \frac{f^s}{R} \right\rangle \operatorname{sign}(\tau^s - x^s)$$

This model has turned out to be computationally very efficient for massive computations of polycrystalline aggregates under cyclic loading, see [17].

## References


[1] M. Hollenstein, M. Jabareen, M. Rubin, *Modeling a smooth elastic-inelastic transition with a strongly objective numerical integrator needing no iteration*, Computational Mechanics **52** (2013), 649–667.

[2] M. Hollenstein, M. Jabareen, M. Rubin, *Erratum to: Modeling a smooth elastic-inelastic transition with a strongly objective numerical integrator needing no iteration*, Computational Mechanics **55** (2015), 453.

[3] M. Rubin, M. Rodríguez-Martínez, *Influence of unobservable overstress in a rate-independent inelastic loading curve on dynamic necking of a bar*, Mechanics of Materials **116** (2018), 158–168.

[4] M. B. Rubin, S. Forest, *Analysis of material instability of a smooth elastic-inelastic transition model*, International Journal of Solids and Structures **193–194** (2020), 39–53.

[5] J. Mandel, *Généralisation de la théorie de plasticité de W.T. Koiter*, International Journal of Solids and Structures **1** (1965), 273–295.
[6] E. Busso, G. Cailletaud, *On the selection of active slip systems in crystal plasticity*, International Journal of Plasticity **21** (2005), 2212–2231.
[7] R. Fortunier, *Dual potentials and extremum work principles in single-crystal plasticity*, Journal of the Mechanics and Physics of Solids **37** (1989), 779–790.
[8] E. Patoor, D. Lagoudas, P. Entchev, L. Brinson, X. Gao, *Shape memory alloys, Part I: General properties and modeling of single crystals*, Mechanics of Materials **38** (2006), 391–429.
[9] M. Arminjon, *A regular form of the Schmid law. Application to the ambiguity problem*, Textures and Microstructures **14–18** (1991), 1121–1128.
[10] W. Gambin, *Crystal plasticity based on yield surfaces with rounded-off corners*, Zeitschrift für Angewandte Mathematik und Mechanik **71** (1991), T265–T268.
[11] T. Kaiser, A. Menzel, *A dislocation density tensor-based crystal plasticity framework*, Journal of the Mechanics and Physics of Solids **131** (2019), 276–302.
[12] L. Anand, M. Kothari, *A computational procedure for rate-independent crystal plasticity*, Journal of the Mechanics and Physics of Solids **44** (1996), 525–558.
[13] C. Miehe, J. Schröder, J. Schotte, *Computational homogenization analysis in finite plasticity simulation of texture development in polycrystalline materials*, Computer Methods in Applied Mechanics and Engineering **171** (1999), 387–418.
[14] L. Scheunemann, P. Nigro, J. Schröder, P. Pimenta, *A novel algorithm for rate independent small strain crystal plasticity based on the infeasible primal-dual interior point method*, International Journal of Plasticity **124** (2020), 1–19.
[15] M. Schurig, A. Bertram, *A rate independent approach to crystal plasticity with a power law*, Computational Materials Science **26** (2003), 154–158.
[16] S. Forest, M. B. Rubin, *A rate-independent crystal plasticity model with a smooth elastic–plastic transition and no slip indeterminacy*, European Journal of Mechanics A/Solids **55** (2016), 278–288.
[17] H. Farooq, G. Cailletaud, S. Forest, D. Ryckelynck, *Crystal plasticity modeling of the cyclic behavior of polycrystalline aggregates under non-symmetric uniaxial loading: Global and local analyses*, International Journal of Plasticity **126** (2019), 102619.

## Cavitation as a fracture event

Gilles A. Francfort
(joint work with A. Giacomini, O. Lopez-Pamies)

The view of cavitation as an elastic phenomenon found its root in the poker-chip experiment of A.N. Gent & P.B. Lindley [4] and was promoted and argued for by J.M. Ball [1]. In their view, point defects expand spherically like $x/|x|$. This forces slow growth of the elastic energy at large strains when adopting the Ball viewpoint that elastic solutions are global minimizers of the potential energy of the system.

As remarked early on most notably by M.L. Williams & R.A. Schapery [9] doing so results in extremely high elastic strains along the boundary of the cavity. Going from an invisible defect (so one of sub-micron size if using electron-microscopy) to a typical 10 micron hole, one would observe bi-axial stretches of the order of $10^2$ to $10^3$ on the surface of the cavity. But polymer chains cannot

stretch to such an extent. Consequently, they suggested to complement the Gent-Lindley picture by accounting for the possible breakage of the crosslinks. This landed with a big thud in the "rubber" world.
A particle filler experiment of A.N. Gent & B. Park [5] was recently revisited by K. Ravi-Chandar [6] and the resulting picture, while vindicating the concepts put forth by Williams and Schapery, calls for a more intricate picture. Indeed, healing occurs, even during the loading phase of a loading cycle. Further, cavities appear in regions of high hydrostatic stress and 0 strain, most likely because of incompressibility. Finally, some kind of hardening phenomenon prevents cavities from reappearing at prior nucleation and propagation sites.
So it seems that cavitation is not only a fracture event, but further, one that is ruled by a non-trivial interplay between elasticity, fracture, incompressibility and hardening. A tall order indeed.
If focussing solely on healing, one can come up with a simple model, assuming, which is most likely not so, that energy is recovered through healing the way it is lost through cracking. In 2D, the energetics is as follows: when going from a crack $K$ to a crack $S$ one should pay (dissipate) $\beta\mathcal{H}^1(S \setminus K)$ and recover $\alpha\mathcal{H}^1(K \setminus S)$ with $\beta > \alpha > 0$ so that there is a net loss (an entropy increase). This is surely an overly simplistic view because it ignores many essential features, but it already tests our current mathematical abilities.
In any case, within this framework one can propose a Griffith-type model which goes roughly as follows for a connected crack $\Gamma(\ell)$ of length $\ell$ at time $t$ along a prescribed crack path $\Gamma \supset \Gamma(\ell)$ in a domain $\Omega$. If, for a given set of boundary conditions on $\partial\Omega$ and time-dependent loads, $\mathcal{P}(t,\ell)$ denotes the potential energy at time $t$ for the crack $\Gamma(\ell)$ associated with the solution of the elasticity problem on the uncracked part of the domain $\Omega \setminus \Gamma(\ell)$ , then the crack evolution – the crack length $\ell(t)$ at time $t$ – is governed by

$$\alpha \leq -\frac{\partial \mathcal{P}}{\partial \ell}(t,\ell(t)) \leq \beta$$
$$-\frac{\partial \mathcal{P}}{\partial \ell}(t,\ell(t)) = \beta, \text{ if } \dot{\ell}(t) > 0$$
$$-\frac{\partial \mathcal{P}}{\partial \ell}(t,\ell(t)) = \alpha, \text{ if } \dot{\ell}(t) < 0.$$

In [3] we demonstrate the existence of a well posed quasi-static energetic evolution à la A. Mielke [7] for the variational rendering of the formulation set forth above under the further topological restriction that the cracks be continua of finite length (compactly connected, or maybe with a preset number of connected components). This is an existence result in the spirit of the original 2D existence result for fracture evolution by G. Dal Maso & R. Toader for fracture only [2]. The precise result was the topic of a previous talk at Oberwolfach; we refer the interested reader to Report No. 33/2017 or, for more details to [3].
We do not know at present how to account for the other ingredients like incompressibility. However, if we adopt a phase field approach, then doing so becomes possible as demonstrated in [8]. Of course, there is a price to pay. We do not know

whether the proposed model converges in any sense to a sharp interface model as the size of the process zone vanishes.

## References


[1] J. M. Ball, *Discontinuous equilibrium solutions and cavitation in nonlinear elasticity*, Philos. Trans. Roy. Soc. London Ser. A **306**, (1982) 557–611.

[2] G. Dal Maso, R. Toader, *A model for the quasi-static growth of brittle fractures: existence and approximation results*, Arch. Ration. Mech. Anal. **162**(2) (2002), 101–135.

[3] G. A. Francfort, A. Giacomini, O. Lopez-Pamies, *Fracture with healing: A first step towards a new view of cavitation*, Analysis and PDE **12**(2) (2019), 417–447.

[4] A. N. Gent, P. B. Lindley, *Internal rupture of bonded rubber cylinders in tension*, Proc. Royal Soc. London **2A** (1959), 195–205.

[5] A. N. Gent, B. Park, *Failure processes in elastomers at or near a rigid inclusion*, J. Mater. Sci. **19** (1984), 1947–1956.

[6] V. Lefèvre, K. Ravi-Chandar, O. Lopez-Pamies, *Cavitation in rubber: An elastic instability or a fracture phenomenon?*, Int. J. Fracture **192** (2015), 1–23.

[7] A. Mielke, *Evolution of rate-independent systems*, In: Evolutionary equations Vol. II, Handb. Differ. Equ., pp. 461–559, A. Dafermos, E. Feireisl (eds), Elsevier/North-Holland, Amsterdam, 2005.

[8] A. Kumar, G. A. Francfort, O. Lopez-Pamies *Fracture and healing of elastomers: A phase-transition theory and numerical implementation*, J. Mech. and Phys. Solids **112** (2018), 523–551.

[9] M. L. Williams, R. A. Schapery, *Spherical flaw instability in hydrostatic tension*, Int. J. Fract. Mech. **1** (1965), 64–71.


## Continuum dislocation dynamics: A mathematical framework for developing a dislocation-based crystal plasticity theory

Anter El-Azab and Thomas Hochrainer

Understanding the strength of metals has been a scientific challenge for many decades. In recent years, much progress was made toward understanding the plastic strength of metals, thanks to the method of dislocation dynamics simulations. This method proved to be powerful for understanding the mechanism of deformation at small strains (about a few percent). Practical levels of crystal deformation encountered in experiments require the development of dislocation based theories of plasticity that capture the deformation mechanisms over a much larger range of strain. The method of continuum dislocation dynamics (CDD) is believed to meet this objective. The method casts the dislocations dynamics problem in the form of transport-reaction equations for crystal dislocations after expressing them in terms of density fields. At this point, however, the method faces theoretical challenges, including modeling of dislocation reactions, collective dislocation mobility, short range interactions, and accounting for the finite deformation kinematics in its mathematical formulation.

The current presentation provided an overview of the current state of CDD modelling, mostly based on the evolution of dislocation density vector fields $\boldsymbol{\rho}^{\mathrm{s}}$ tied to slip systems $s$. In this case the dislocation vector fields are supposed to provide a complete characterization of the dislocation state. The density fields characterize

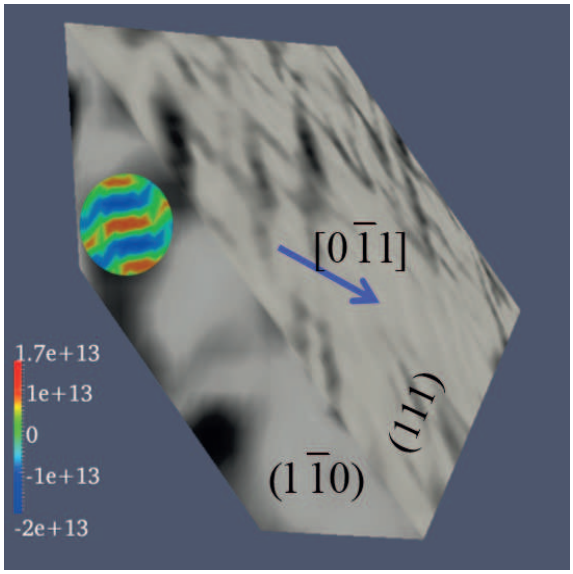


FIGURE 1. Dislocation vein structure developing in CDD simulations of cyclic loading. Grayscale depicts total dislocation density. Color inlet shows alternating edge-component in the wall.

a distribution of curves. Given a dislocation velocity vector field $\boldsymbol{v}^{\mathrm{s}}$ of these curves, the evolution equations of the density fields are given by balance laws of the form

$$\dot{\boldsymbol{\rho}}^{\mathrm{s}} = \operatorname{curl}\left(\boldsymbol{v}^{\mathrm{s}} \times \boldsymbol{\rho}^{\mathrm{s}}\right) + \dot{\boldsymbol{\rho}}^{\mathrm{s}}_{\mathrm{net}}\,, \tag{1}$$

in small deformation formulation. The curl-term represents the pure transport of line-density, while the network term $\dot{\boldsymbol{\rho}}^{\mathrm{s}}_{\mathrm{net}}$ may represent a multitude of dislocation reactions [1] (typically involving other slip systems) which affect the evolution of the dislocation network. The network term was recently adapted to consider cross-slip and various dislocation reactions, including collinear reactions and glissile reactions, which recently received increased attention due to findings in discrete dislocation simulations. The power of such CDD formulations was demonstrated by revealing the origin of dislocation cell structure formation and hardening behavior in FCC crystals. Figure 1 exemplarily shows a vein structure that consists of dislocation walls perpendicular to the Burgers vectors, which developed in CDD simulations of cyclic loading. The color inlet shows the (signed) edge-component of the dislocation density, which demonstrates the dipolar nature of the walls.
Besides the progress towards including dislocation reactions into CDD we also discussed recent reformulations of CDD in the large deformation framework of multiplicative crystal plasticity [2]; when the deformation gradient $\boldsymbol{F}$ is decomposed as $\boldsymbol{F} = \boldsymbol{F}^{\mathrm{e}}\boldsymbol{F}^{\mathrm{p}}$ into an elastic and a plastic part. It was shown that large deformation kinematics applied to evolving fields of tensorial dislocation densities accounts for kinking and jogging of dislocations when cutting through one another. This may be best seen when dislocation density vector fields are defined on the intermediate (or isoclinic) configuration. On this configuration the evolution equation for the dislocation density vector takes the form (neglecting a possible

network term)

$$\dot{\boldsymbol{\rho}}^{\mathrm{s}} = \mathrm{curl}^{\mathrm{p}}\left(\boldsymbol{v}^{\mathrm{s}} \times \boldsymbol{\rho}^{\mathrm{s}}\right) + \boldsymbol{L}^{\mathrm{p}}\boldsymbol{\rho}^{\mathrm{s}} - \mathrm{tr}\left(\boldsymbol{L}^{\mathrm{p}}\right)\boldsymbol{\rho}^{\mathrm{s}}\,, \tag{2}$$

where $\boldsymbol{L}^{\mathrm{p}}$ denotes the rate of plastic distortion tensor, such that $\dot{\boldsymbol{F}}^{\mathrm{p}} = \boldsymbol{L}^{\mathrm{p}}\boldsymbol{F}^{\mathrm{p}}$. Furthermore, $\mathrm{curl}^{\mathrm{p}}$ denotes the curl-operator on the intermediate configuration. Equation (2) entails that the dislocation vector fields $\boldsymbol{\rho}^{\mathrm{s}}$ do not remain planar vector fields in the slip planes, such that multiple slip deformation will necessarily involve non-conservative motion of jogged dislocations. Because non-conservative dislocation motion in crystals is only possible through the creation or destruction of point-defects, large deformation CDD needs to be coupled to evolving fields of point defects; most notably vacancies. Such a theory opens new persepctives for modelling various phenomena in metal physics and plasticity which are tied to high point defect densities, e.g., strain hardening, creep, hydrogen embrittlement, or ductile fracture.

## References

[1] P. Lin, A. El-Azab, *Implementation of annihilation and junction reactions in vector density-based continuum dislocation dynamics*, accepted for publication in MSMSE, (2020).

[2] T. Hochrainer, B. Weger, *Is Crystal Plasticity Non-Conservative? Lessons from Large Deformation Continuum Dislocation Theory*, under review at JMPS, (2020).

## Phase-field modeling of fracture – heterogeneities and cyclic loadings

Markus Kästner

(joint work with Franz G. Dammaß, Arne C. Hansen-Dörr, Martha L. Seiler)

The phase-field method has become a powerful tool for the modelling of fracture. Due to the diffuse representation of the crack, topological updates of the analysis mesh are avoided which is particularly helpful for the analysis of complex crack patterns and three-dimensional problems. Recent developments of the method involve the representation of fracture in heterogeneous solids and the numerically efficient consideration of cyclic loadings. In this contribution, both problems are addressed in terms of modifications of the fracture toughness $\mathcal{G}_{\mathrm{c}}$.

### 1. Heterogeneities

In heterogeneous material, e.g. composites, interfaces play a crucial role in component failure. Here, a phase-field model for brittle fracture is combined with a diffuse representation of the microstructure. In particular, the fracture toughness $\mathcal{G}_{\mathrm{c}}\left(\boldsymbol{x}\right)$ is reduced in the vicinity of an interface

$$\mathit{\Pi} = \int_{\Omega} (1-d)^2\psi_{+}^{\mathrm{el}} + \psi_{-}^{\mathrm{el}}\,\mathrm{d}V + \int_{\Omega} \mathcal{G}_{\mathrm{c}}\left(\boldsymbol{x}\right)\frac{1}{2\ell}(d^2 + \ell^2|\nabla d|^2)\,\mathrm{d}V\ . \tag{1}$$

It is shown that the regularisations of crack in terms of the phase-field order parameter $d$ with the characteristic length $\ell$ and a diffuse interface of width $\ell_{\mathrm{i}}$ interact which has to be compensated [1]. The approach is compared to and validated for an example from linear elastic fracture mechanics [2], Fig. 1.

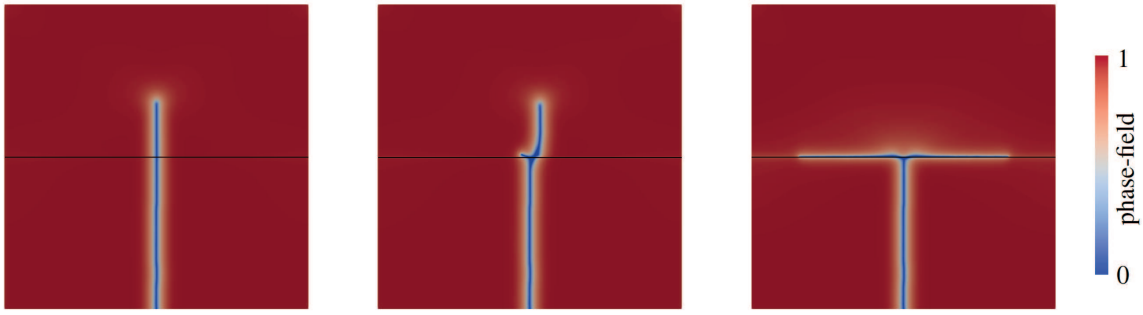


(a) $\mathcal{G}_c^b/\mathcal{G}_c^i = 4.5$ (b) $\mathcal{G}_c^b/\mathcal{G}_c^i = 4.75$ (c) $\mathcal{G}_c^b/\mathcal{G}_c^i = 6$

FIGURE 1. Initial crack perpendicular to an interface under mode I loading (horizontal direction): In line with linear elastic fracture mechanics, three different phenomena **(a)** – **(c)** are predicted depending on the ratio $\mathcal{G}_c^b/\mathcal{G}_c^i$ of bulk and interface fracture toughnesses. The midline of the regularised weak interface is indicated in black.

## 2. Fatigue crack growth

As fatigue comes along with high numbers of load cycles, a direct simulation of the loading history [3] is computationally expensive, especially for inelastic material behaviour. To this end, we combine the phase-field method for brittle fracture with the notch strain concept. The standard phase-field formulation is extended to fatigue crack growth by a fracture toughness $\mathcal{G}_c(D)$ that depends on a lifetime variable $D$ [4]

$$\Pi = \int_\Omega g(d)\,\psi^e(\boldsymbol{\varepsilon})\,\mathrm{d}V + \int_\Omega \mathcal{G}_c\,(D)\,\frac{1}{2\ell}(d^2 + \ell^2|\nabla d|^2)\,\mathrm{d}V\ . \tag{2}$$

For $D = 0$ a material point has experienced no fatigue loads at all, while $D = 1$ means it has undergone all load cycles it can possibly bear before loosing its integrity. The lifetime variable $D$ is determined with the local strain concept and is associated to cyclic plasticity in the vicinity of the crack determined by Neuber's rule. The method is tested with a compact tension (CT) test. In Fig. 2, the evolution of the crack $d$ and of the zone of cyclic plasticity $D$ are illustrated.

## References

[1] A. C. Hansen-Dörr, P. Hennig, R. de Borst, M. Kästner, *Phase-field modeling of interface failure in brittle materials*, Comput. Methods in Appl. Mech. Eng. **346** (2018), 25–42.

[2] A. C. Hansen-Dörr, F. G. Dammaß, R. de Borst, M. Kästner, *Phase-field modeling of crack branching and deflection in heterogeneous media*, accepted in Eng. Fract. Mech. (2020), arXiv preprint arXiv:1910.08277.

[3] P. Carrara, M. Ambati, R. Alessi, L. De Lorenzis, *A framework to model the fatigue behavior of brittle materials based on a variational phase-field approach*, Comput. Methods in Appl. Mech. Eng. **361** (2019), 112731.

[4] M. Seiler, T. Linse, P. Hantschke, M. Kästner, *An efficient phase-field model for fatigue fracture in ductile materials*, Eng. Fract. Mech. **224** (2020), 106807.

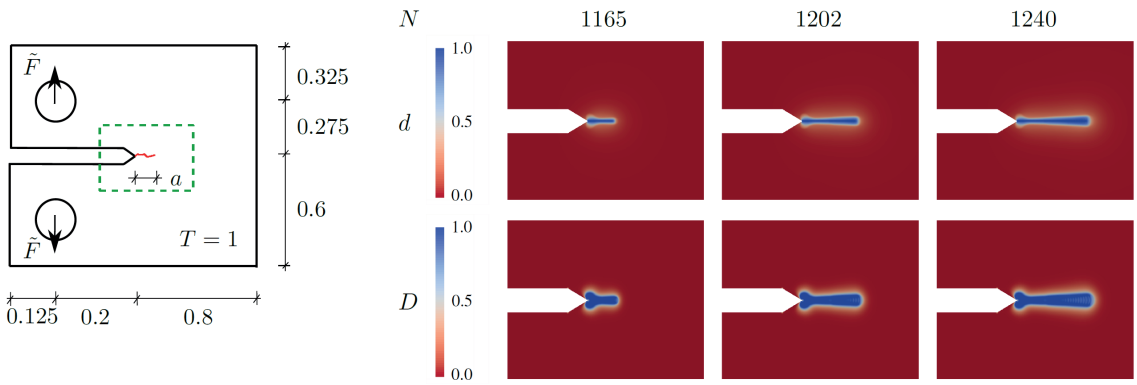


FIGURE 2. Compact tension test: Evolution of phase-field variable $d$ and lifetime variable $D$ for load cycles $N$.

## Achievements and open challenges in modeling microstructure evolution in magnetizable solids via energy relaxation

BJOERN KIEFER

(joint work with Thorsten Bartel, Andreas Menzel)

Magnetic shape memory alloys (MSMA) are an ideal model material to study the interplay of microstructure evolution and effective magnetomechanical response characteristics. Microstructure in this case refers to twinned variants with internal domain structures in ferromagnetic martensites. After initially pursuing MSMA modeling in the tradition of plasticity-like models for conventional thermal SMA [11], a fundamentally different approach was taken by the authors in recent years, in following concepts of energy relaxation, for which much experience also already existed in the group [3].

The relaxation approach centers on describing stable effective material behavior by computing convex hulls (of different variety) to multi-well energy landscapes. Microstructure formation can in this context be interpreted as material instability on the lower scale. As a point of departure for employing this method in the context of magnetomechanical coupling, the constrained theory of magnetoelasticity was studied [7], which comprises elements of micromagnetics theory [4] and the Ball and James theory on martensitic microstructures as minimizers of energy [1]. It was also demonstrated, however, that some of the restrictions of such a model are so severe that they contradict experimental observations and consequently elastic straining, magnetization rotations—i.e. deviations from the energetic minima—as well as dissipation must be included in the constitutive model to capture the characteristic of MSMA responses.

There are several distinct advantages to the relaxation modeling approach for MSMA, see [10, 2]. Both the parameter set and the microstructural variables consist of physically well-motivated and easily interpretable quantities. Moreover, all key mechanisms may occur simultaneously and in arbitrary combinations or order. The model obeys a single physical principle, i.e. stationarity of an energy

functional, with no need for purely phenomenological evolution equations. The microstructure formation at each material point is influenced by the magnetostatic energy stored in the entire self-field [5]. The theoretical foundation of the approach is strongly supported by mathematical analysis, related to the existence of minimizers for the underlying variational problems [1, 6, 7]—although more work is needed to fully analyze the extended formulation. The model captures all key response features characteristic of single crystalline MSMA behavior (e.g. nonlinear, anisotropic, stress-level and loading history-dependent magnetic field-induced strain and magnetization responses, magnetic field-biased pseudoelasticity etc.) and its predictions have been validated by experiments—where relevant data was available. Finally, the relaxation-based modeling framework is so general that it can be applied to many other cases of microstructure-driven magnetomechanical material behavior, such as observed in giant magnetostrictives [7].
A caveat to the current formulation is the fact that relaxation is, strictly speaking, only applied w.r.t. mechanical degrees of freedom—although minimization of a fully-coupled functional is conducted. No regard is currently given, however, to the interface compatibility of magnetic field variables during relaxation. On the other hand, we were recently able to show that concepts analogous to rank-one convexification can be established for the purely magnetic case [9]. An open question is therefore how to combine these concepts and whether relaxation in the coupled case ought to be carried out in monolithic or rather staggered fashion, in the sense of sequential partial relaxations. Some interesting discussions to this end were held during the Oberwolfach workshop, in which generalized concepts of relaxation [8] were pointed out by colleagues of the mathematics community, as one possible avenue of future investigation in this regard.

## Acknowledgements

The financial support by the German Research Foundation (DFG) through the Research Unit 1509: "Ferroic Functional Materials: Multi-Scale Modeling and Experimental Characterization", projects P6 (ME 1745/8-2) and P7 (KI 1392/4-2, BA 4195/2-2), is gratefully acknowledged.

## References

[1] J. M. Ball and R. D. James, *Fine phase mixtures as minimizers of energy*, Arch. Ration. Mech. Anal. **100** (1987), 13–52.

[2] T. Bartel, B. Kiefer, K. Buckmann, A. Menzel, *An energy-relaxation-based framework for the modelling of magnetic shape memory alloys — simulation of key response features under homogeneous loading conditions*, Int. J. Solids Struct. **182–183** (2020), 162–178.

[3] T. Bartel, A. Menzel, B. Svendsen, *Thermodynamic and relaxation-based modeling of the interaction between martensitic phase transformations and plasticity*, J. Mech. Phys. Solids **59** (2011), 1004–1019.

[4] W. F. Brown, Jr., *Micromagnetics*, vol. 18 of Interscience Tracts on Physics and Astronomy (1963), John Wiley & Sons, New York.

[5] K. Buckmann, B. Kiefer, T. Bartel, A. Menzel, *Simulation of magnetised microstructure evolution based on a micromagnetics-inspired FE-framework: Application to magnetic shape memory behaviour*, Arch. Appl. Mech. **89** (2019), 1085–1102.

[6] A. DeSimone, *Energy minimizers for large ferromagnetic bodies*, Arch. Ration. Mech. Anal. **125** (1993), 99–143.
[7] A. DeSimone, R. D. James, *A constrained theory of magnetoelasticity.*, J. Mech. Phys. Solids **50** (2002), 283–320.
[8] I. Fonseca, S. Müller, *$\mathcal{A}$-quasiconvexity, lower semiconinuity, and young measures*, SIAM J. Math. Anal. **30** (1999), 1355–1390.
[9] B. Kiefer, T. Bartel, *On variationally-consistent homogenization approaches in multi-phase magnetic solids*, Proc. Appl. Math. Mech. **17** (2017), 517–518.
[10] B. Kiefer, K. Buckmann, T. Bartel, *Numerical energy relaxation to model microstructure evolution in functional magnetic materials*, GAMM-Mitteilungen **38** (2015), 171–196.
[11] B. Kiefer, D. C. Lagoudas, *Modeling the coupled strain and magnetization response of magnetic shape memory alloys under magnetomechanical loading*, J. Intel. Mat. Syst. Str. **20** (2009), 143–170.

## Uniform-approximation approach vs. Vekua-type approximation

Reinhold Kienzler
(joint work with Patrick Schneider)

The three-dimensional continuum theory of elasticity can be derived in a mathematically rigorous way from first principles. In contrast, theories for thin structures, that are modeled by differential equations on one- or two-dimensional domains, can only be approximations of the three-dimensional theory. The treatment of a structural element as a thin structural member comes always along with a systematic error, even if the modeling equations are solved exactly. Although there is a vast amount of literature concerning theories (mathematical models) for thin structural members, only for very few models there exist justifications in the sense of a mathematical proof that the systematic error is actually converging to zero if the structure gets thinner.

The uniform-approximation approach is a structured, constructive approach for the derivation of lower-dimensional analytical theories for thin structural members from the three-dimensional theory of elasticity. It has been successfully applied to a variety of problems by numerous authors. The justification of the approach in the form of an order of magnitude estimate for the systematic error, using a duality principle, was recently provided in [1].

After the insertion of a suitable series expansion of the displacement field, the elastic potential takes the form of a power series-expansion in a dimensionless parameter that describes the relative thinness of the structure. The approach delivers hierarchies of theories by truncating the elastic potential after a certain power of the dimensionless parameter, which defines the order of approximation for the uniform-approximation approach.

It has been shown that the first-order approximations for isotropic material deliver the known classical theories, like the Kirchhoff plate theory, or the Euler-Bernoulli beam theory, without invoking a-priori assumptions [2]. This is also in accordance with results using different justification approaches. On the other hand, due to its constructive nature, the uniform-approximation approach also allows to derive extended refined theories and/or theories for anisotropic materials in a systematic

way, like demonstrated by the authors for the case of a Reissner-type plate theory for monoclinic material [3, 4].
In contrast to the uniform-approximation approach, the in the engineering literature most used structured approach, here called Vekua-type approach, generates approximate theories by replacing the infinite series expansion of the displacement field by a fixed finite sum [5]. Here the order of approximation is usually defined as the order of the finite displacement ansatz.
In the talk, we used standard arguments from duality theory to derive a priori error estimates of the systematic error of solutions of the so-derived approximate theories in comparison to the exact solution of three-dimensional elasticity. Both approaches achieve convergence in a weak-solution sense.
Comparing the magnitudes of the energetic summands that are considered for both approaches, we find that the geometric scaling factors describing the relative thinness of the structure, that are used to truncate the energy series in the case of the uniform approximation approach, initially dominate the decaying behavior, whereas, the Vekua-type approach is favorable for asymptotic investigations.
However, in practice, there is no demand for arbitrary high precision: After a certain threshold a further increase of precision will be irrelevant for practical applications. We show that even for not at all thin structures, the geometric scaling factors clearly still dominate the decaying behavior in the regime of technical relevant precision. Furthermore, we show that for a given precision, the Vekua-type theory achieving this precision has in general a more complex modeling partial differential equation (PDE) system than the uniform theory. Therefore, the Vekua-type approach is considered suboptimal by the present authors. In addition, the uniform theories' PDE systems are better suited for so-called pseudo reductions, which are transformations that reduce the number of PDEs in the system as well as the number of unknowns at the cost of higher-order PDEs. All details about the error estimate as well as the comparison of the approaches can be found in [1].

## References

[1] P. Schneider, R. Kienzler, *A priori estimation of the systematic error of consistently derived theories for thin structures*, International Journal of Solids and Structures **190** (2020), 1–21, Doi: 10.1016/j.ijsolstr.2019.10.010.

[2] R. Kienzler, P. Schneider, *A beam - Just a beam in linear plane bending*, in H. Altenbach, J. Chróścielewski, V. Eremeyev, & K. Wiśniewsju (Eds.), *Recent Developments in the Theory of Shells*, volume 110, Springer, Cham, 2018, 329–350, Doi: 10.1007/978-3-030-17747-8-18.

[3] P. Schneider, R. Kienzler, M. Böhm, *Modeling of consistent second-order plate theories for anisotropic materials*, ZAMM - Journal of Applied Mathematics and Mechanics **94**(1–2) (2014), 21–42, Doi: 10.1002/zamm.201100033.

[4] P. Schneider, R. Kienzler, *A Reissner-type plate theory for monoclinic material derived by extending the uniform-approximation technique by orthogonal tensor decompositions of nth-order gradients*, Meccanica **52**(9) (2017), 2143–2167, Doi: 10.1007/s11012-016-0573-1.

[5] P. Schneider, R. Kienzler, *Comparison of various linear plate theories in the light of a consistent second-order approximation*, Mathematics and Mechanics of Solids **20**(7) (2014), 871–882, Doi: 10.1177/1081286514554352.

## A scale adaptive FE$^2$ method for the analysis of the non-linear thermo-mechanical coupled behavior of a fiber reinforced material

Sven Klinkel
(joint work with Maximilian Praster)

The contribution deals with the multiscale analysis of a reinforced matrix with shape-memory-alloy (SMA) fibers. With respect to the assumption of scale separation, the problem is simulated with the FE$^2$ approach, see [1]. The mechanical behavior of the micro structure, which consists of a linear-elastic matrix and a random fiber distribution, is captured by a representative volume element (RVE). The SMA fibers are characterized by a highly non-linear, thermo-mechanically coupled material behavior. The nonlinear behavior of the macroscopic structure depends on the deformation, the SMA fiber orientation and the temperature of the micro scale. This necessitates an accompanying homogenization to capture the macroscopic stress and stiffness during the loading of the structure. Therefore, the FE$^2$ method is employed. It solves two nested boundary value problems (BVP) on the micro and on the macro scale. The BVP of the micro scale is solved at every integration point of the macroscopic problem in each iteration step. This makes the FE$^2$ method computational expensive. The purpose of the present work is to reduce the computational effort by introducing an indicator for the multiscale analysis. The accompanying homogenization is only performed if the indicator predicts nonlinear behavior on the micro structure. The SMA in the micro structure will stay linear elastic until the phase transition condition is reached, which is defined by a critical temperature dependent stress state. It motivates the introduction of an indicator on the macro scale, which is defined as a critical temperature dependent strain state, see also [2]. A strain state above the limit strain indicates that an accompanying homogenization at the integration point is necessary. Therefore, Dirichlet boundary conditions are employed for the underlying RVE. In the initial iteration step of the first load step the homogenization is performed by assuming Neumann boundary conditions for the underlying RVE.

A numerical example demonstrates the capability of the present approach. The Cook membrane with an uniformly distributed load and randomly oriented SMA fibers is analyzed. The system and loading are illustrated in Fig. 1. The matrix is assumed to be linear elastic, whereas the fibers have non-linear temperature dependent behavior. The fibers are randomly oriented.

The representative volume element is modeled by $20 \times 20$ elements. The Cook membrane is discretized by 400 elements. The temperature is assumed to be linear distributed from the left to the right from 255 K to 270 K. The load $F$ is increased form $F = 0$ up to $F = 20$ in 20 load steps. For each load step the indicator is employed to decide weather an embedded numerical homogenization is possible or not. In Fig. 2 the identified elements with an embedded homogenization are shown for two load levels. Especially at the beginning of the loading the accompanying homogenization is not necessary for the most of the elements. In comparison to the situation where all elements have a nested homogenization the present approach

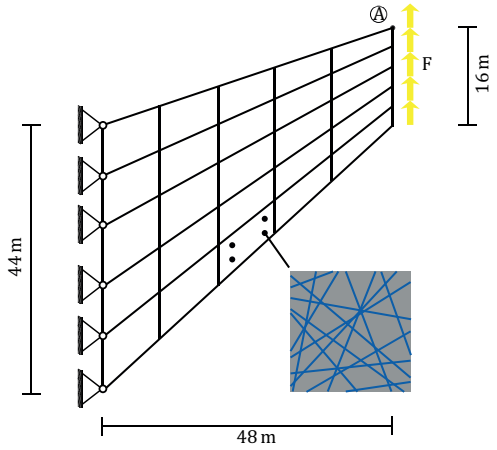


FIGURE 1. Cook membrane, loading and system with randomly oriented fibers with a volume fraction of 10%

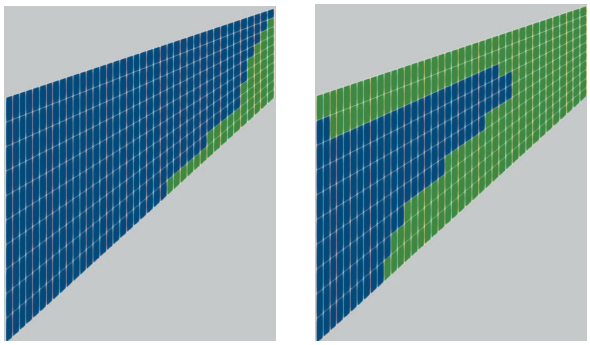

FIGURE 2. Illustration of elements with (green) and without (blue) a nested homogenization for F=10 (left) and F=20 (right)

saves some computational cost. The difference of the maximum displacement of the present approach and the situation, where a nested homogenization is considered in all elements, depends on the load level and is in-between 5% and 0%.

## REFERENCES

[1] F. Feyel, J. L. Chaboche *$FE^2$ multiscale approach for modelling the elastoviscoplastic behaviour of long fibre SiC/Ti composite materials*, Computational Methods in Applied Mechanics and Engineering **183** (2000), 309.

[2] M. Praster, M. Klassen, S. Klinkel, *An adaptive $FE^2$ approach for fiber-matrix composites*, Computational Mechanics **63** (2019), 1333–1350.

# Fracture and damage models as rate-independent systems

Dorothee Knees

## 1. Short overview on solution concepts for rate-independent systems

Within certain regimes the behavior of dissipative solids can be considered as rate-independent. Rate-independence means that after rescaling the loads in time the solutions to the system with the new loads are exactly the rescaled solutions of the original system. Phenomena like plasticity, damage and fracture of brittle materials or the shape memory effect can be modeled in this framework. Following the frame of standard generalized materials, [4], one assumes that the state of a mechanical structure is completely characterized by a displacement (or deformation) field $u$ belonging to a state space $\mathcal{U}$ and internal variables $z \in \mathcal{Z}$. The latter for instance encode the plastic strains, the damage state or the polarization in ferroelectric materials. Due to constraints like the flow rule in plasticity or the Griffith fracture criterion the resulting system in general consists of a (quasistatic) balance of linear momentum and a nonsmooth evolution inclusion: Given a time dependent load $\ell : [0,T] \to \mathcal{U}^*$ and an initial state $z_0 \in \mathcal{Z}$ the task is to determine $u : [0,T] \to \mathcal{U}$ and $z : [0,T] \to \mathcal{Z}$ with $z(0) = z_0$ satisfying for (almost all) $t$

$$\ell(t) = \mathrm{D}_u \mathcal{E}(u(t), z(t)), \tag{1}$$

$$0 \in \partial \mathcal{R}(\dot{z}(t)) + \mathrm{D}_z \mathcal{E}(u(t), z(t))\,. \tag{2}$$

Here, $\mathcal{E} : \mathcal{U} \times \mathcal{Z} \to \mathbb{R}$ is the stored energy functional and $\mathcal{R} : \mathcal{Z} \to [0,\infty]$ is a convex pseudo dissipation potential with $\mathcal{R}(0) = 0$. In the rate-independent case it is assumed that $\mathcal{R}$ is positively homogeneous of degree one. $\mathrm{D}_u \mathcal{E}(\cdot)$ and $\mathrm{D}_z \mathcal{E}(\cdot)$ are the variational derivatives of $\mathcal{E}$ with respect to $u$ and $z$, while $\partial \mathcal{R}$ denotes the subdifferential of $\mathcal{R}$.

In many applications, in particular in the modeling of damage and fracture, the stored energy functional $\mathcal{E}$ is not convex. In this case, the system (1)–(2) in general does not admit global in time continuous solutions, even if the applied loads are smooth in time. We illustrate this observation in Section 2 with an example. Hence, one either has to resort to a local existence theory or one has to interpret the system (1)–(2) in a weak form that also admits discontinuous solutions. In this way, the system is enriched with jump criteria. There are several different ways of defining weak solutions for rate-independent systems. Note that they are not equivalent and that the jump criteria introduced are not the same. From the point of view of applications this is a severe problem since according to one weak solution concept a structure might be safe while according to a different solution concept the structure might fail given the same loads.

In the last twenty years, two main solution concepts were developed: (global) energetic solutions and vanishing viscosity solutions. We refer to [15] for an overview.

**Energetic solutions** are characterized by a global stability condition and an energy dissipation balance that both have to be satisfied for all $t \in [0,T]$:

$$\forall (v,\zeta) \in \mathcal{U} \times \mathcal{Z} \qquad \widetilde{\mathcal{E}}(t,u(t),z(t)) \le \widetilde{\mathcal{E}}(t,v,\zeta) + \mathcal{R}(\zeta - z(t)), \tag{3}$$

$$\widetilde{\mathcal{E}}(t,u(t),z(t)) + \mathrm{Diss}_{\mathcal{R}}(z,[0,t]) = \widetilde{\mathcal{E}}(0,u_0,z_0) - \int_0^t \langle \dot{\ell}(\tau), u(\tau)\rangle \,\mathrm{d}\tau. \tag{4}$$

Here, $\widetilde{\mathcal{E}}(t,u,z) := \mathcal{E}(u,z) - \langle \ell(t), u\rangle$ and

$$\mathrm{Diss}_{\mathcal{R}}(z,[\alpha,\beta]) = \sup_{\text{Partitions of } [\alpha,\beta]} \sum_{\alpha=t_0<\ldots<t_n=\beta} \mathcal{R}(z(t_{i+1}) - z(t_i))$$

denotes the total variation of a curve $z : [\alpha,\beta] \to \mathcal{Z}$ with respect to the dissipation potential $\mathcal{R}$. For many rate-independent mechanical models the existence of energetic solutions was shown, [15]. Since the characterization (3)–(4) involves $\mathcal{E}$ only but not its derivatives, rather mild assumptions on $\mathcal{E}$ are sufficient in order to guarantee the existence of solutions. As a highlight it was possible to prove the existence of solutions to the quasistatic Francfort-Marigo fracture model, [2]. Moreover, this solution concept allows for the application of variational arguments and in particular for the tools from $\Gamma$-convergence theory if one wants to analyze parameter dependent systems and identify effective quantities in scaling limits. However, due to the global minimality condition (3), energetic solutions tend to develop jumps across energy barriers.

**Balanced viscosity solutions** are obtained as vanishing viscosity limits ($\nu \searrow 0$) of viscously regularized rate-independent systems consisting of (1) and

$$0 \in \partial\mathcal{R}(\dot{z}(t)) + \nu\dot{z}(t) + \mathrm{D}_z\mathcal{E}(u(t),z(t)). \tag{5}$$

We will not give here a detailed characterization of balanced viscosity solutions but refer to [13, 6]. Starting from the paper [3] this concept was developed for abstract rate-independent systems (e.g. [13]), and applied to damage models (e.g. [8]), crack propagation models with single cracks (e.g. [10, 12]) and different models in plasticity (e.g. [1]). According to this solution concept, solutions tend to develop discontinuities as late as possible and they do not jump across energy barriers. However, from a mathematical point of view strong structural assumptions have to be formulated for the energy functional $\mathcal{E}$ in order to guarantee the existence of solutions. In particular, certain weak continuity properties on the derivatives of $\mathcal{E}$ are needed. Due to these constraints it is not clear how to apply this solution concept to the Francfort-Marigo fracture model. In addition to these two main concepts further solution concepts were developed in the last years, where for instance solutions are allowed to jump across small energy barriers [11], or where special scalings in the viscosity approach were prescribed (visco-energetic solutions, [16]).

## 2. Example: Propagation of a single crack

The example from [9] illustrates the different predictions of the two main solution concepts. Let $\Omega = (0,10)\times(-1,1) \subset \mathbb{R}^2$ (in cm) be a two dimensional rectangular domain where a single crack may propagate along the line $(0,10)\times\{0\}$ (prescribed crack path) according to the Griffith fracture criterion. The body is occupied by a linear elastic, isotropic material (with $E = 210\text{kN/mm}^2$, $\nu = 0.28$, fracture toughness $\kappa = 50\text{MPa}\,\text{m}^{\frac{1}{2}}$). Non penetration conditions are imposed on the crack faces. Let $\Omega_z := \Omega\backslash\big((0,z)\times\{0\}\big)$ denote the domain with a crack of length $z$. The set of admissible displacements is given by

$$\mathcal{K}(\Omega_z) = \{u \in H^1(\Omega_z,\mathbb{R}^2)\,;\, u = 0 \text{ on } \{10\}\times(-1,1), \quad [u]\cdot\boldsymbol{n} \geq 0 \text{ along the crack }\}\,.$$

On the upper and lower boundary (i.e. on $(0,10)\times\{\pm1\}$), monotone loads are applied of the form $\ell(t) = t\ell_*$ for $t \in [0,T]$ and with a piecewise constant load profile $\ell_*(x) = \pm 0.15$ for $x \in (0,2)\times\{\pm1\}$, $\ell_*(x) = \mp 1$ for $x \in (2,4)\times\{\pm1\}$ and $\ell_*(x) = \pm 1$ for $x \in (4,5)\times\{\pm1\}$. Finally, $\ell_* = 0$ on the remaining parts of the boundary. Clearly, for every $t$ and $z$ there is a unique $u = u(t,z) \in \mathcal{K}(\Omega_z)$ that minimizes $\mathcal{E}(t,\cdot,z)$ with respect to $\mathcal{K}(\Omega_z)$. Let $\mathcal{I}(t,z) := \mathcal{E}(t,u(t,z),z)$ be the reduced functional. The energy release rate $\mathcal{G}(t,z) := -\frac{\mathrm{d}}{\mathrm{d}z}\mathcal{I}(t,z)$ is well defined and we refer to [9, 5] for a short overview on further mathematical properties. Given a fracture toughness $\kappa > 0$ the Griffith fracture criterion characterizes the propagation of the crack as follows:

$$\dot z(t) \geq 0, \quad \mathcal{G}(t,z(t)) \leq \kappa, \quad \dot z(t)\big(\kappa - \mathcal{G}(t,z(t))\big) = 0.$$

In terms of the dissipation functional $\mathcal{R}(v) := \kappa v$ if $v \geq 0$ and $\mathcal{R}(v) = \infty$ for $v < 0$, these conditions can be reformulated as

$$0 \in \partial\mathcal{R}(\dot z(t)) + \mathrm{D}_z\mathcal{I}(t,z(t)),$$

which is (2).

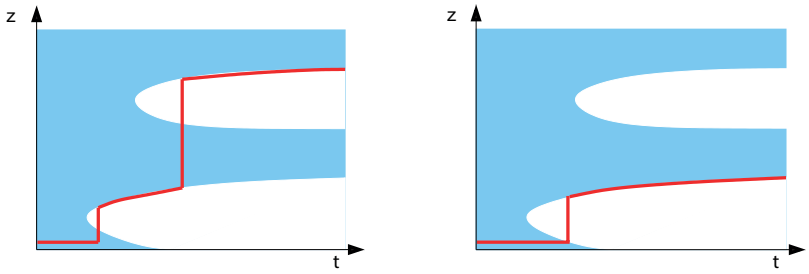


Figure 1. Left: Energetic solution; Right: vanishing viscosity solution; both as functions of time (horizontal axis)

The red curves in Figure 1 show a sketch of the energetic solution (left) and the vanishing viscosity solution (right) for this example. For the precise numerical calculations we refer to [9]. The blue regions in both figures indicate those pairs $(t,z)$ for which $\mathcal{G}(t,z) < \kappa$, while in the white regions we have $\mathcal{G}(t,z) > \kappa$. Observe that the energetic solution develops a first jump although according to the Griffith

criterion the crack should not grow at all. Due to the global minimality condition (3), a second jump appears, where the crack passes through the compressed region in the body and continues to grow afterwards. In contrast to this, the vanishing viscosity solution develops one jump with a subsequent continuous propagation. Observe that at the time instance, where the viscosity solution develops the jump, it is not possible to extend the crack in a continuous way and at the same time respecting the condition $\mathcal{G}(t, z(t)) \leq \kappa$.

## 3. Discussion and questions

The example in the previous section illustrates that the two solution concepts (energetic solutions and vanishing viscosity solutions) are not equivalent and that they predict substantially different jump discontinuities. Such phenomena do not only appear in this particular crack propagation example but they are intrinsic to all rate-independent models with a nonconvex energy $\mathcal{E}$. Let us stress that rate-independent damage models and phase-field fracture models used in practice have these ambiguities. In fact, the choice of the solution class is part of the modeling.

This observation raises the following questions: Which types of solutions are approximated by numerical schemes that are used in practice (e.g. time incremental alternate minimization schemes or staggered schemes)? In [7], this question was investigated for the Ambrosio-Tortorelli damage model. Are there efficient and feasible schemes that reliably approximate that type of solution one is interested in? Some prototypical schemes were analyzed in [6] for a simplified semilinear rate-independent system. Do scaling limits of multi-rate systems help to identify physically reasonable solution classes? Here, we refer to [14] for first answers. What is a good mathematical as well as mechanical framework for the coupling of rate-dependent with rate-independent processes?

## References


[1] G. Dal Maso, A. DeSimone, M. G. Mora, M. Morini, *A vanishing viscosity approach to quasistatic evolution in plasticity with softening*, Archive for Rational Mechanics and Analysis **189** (2008), 469–544.

[2] G. Dal Maso, G. A. Francfort, R. Toader, *Quasistatic crack growth in nonlinear elasticity.*, Arch. Ration. Mech. Anal. **176** (2005), 165–225.

[3] M. A. Efendiev, A. Mielke, *On the rate-independent limit of systems with dry friction and small viscosity*, Journal of Convex Analysis **13** (2006), 151–167.

[4] B. Halphen, N. Q. Son, *Sur les matériaux standards généralisés*, Journal de Mécanique Théorique et Appliquée. Journal of Theoretical and Applied Mechanics **14** (1975), 39–63.

[5] D. Knees, *A short survey on energy release rates*, in Oberwolfach Report, Mini-Workshop: Mathematical Models, Analysis, and Numerical Methods for Dynamic Fracture 2011, G. D. Maso, C. J. Larsen, C. Ortner, eds., EMS.

[6] D. Knees, *Convergence analysis of time-discretisation schemes for rate-independent systems*, ESAIM, Control Optim. Calc. Var. **25**, article 65 (2019).

[7] D. Knees, M. Negri, *Convergence of alternate minimization schemes for phase-field fracture and damage.*, Math. Models Methods Appl. Sci. **27** (2017), 1743–1794.

[8] D. Knees, R. Rossi, C. Zanini, *A vanishing viscosity approach to a rate-independent damage model*, Mathematical Models and Methods in Applied Sciences **23** (2013), 565–616.

[9] D. Knees, A. Schröder, *Computational aspects of quasi-static crack propagation*, Discrete and Continuous Dynamical Systems. Series S **6** (2013), 63–99.
[10] D. Knees, C. Zanini, A. Mielke, *Crack growth in polyconvex materials*, Physica D. Nonlinear Phenomena **239** (2010), 1470–1484.
[11] C. J. Larsen, *Epsilon-stable quasi-static brittle fracture evolution.*, Commun. Pure Appl. Math. **63** (2010), 630–654.
[12] G. Lazzaroni, R. Toader, *A model for crack propagation based on viscous approximation.*, Math. Models Methods Appl. Sci. **21** (2011), 2019–2047.
[13] A. Mielke, R. Rossi, G. Savaré, *Balanced viscosity (BV) solutions to infinite-dimensional rate-independent systems.*, J. Eur. Math. Soc. (JEMS) **18** (2016), 2107–2165.
[14] ———, *Balanced-viscosity solutions for multi-rate systems.*, J. Phys., Conf. Ser. **727** (2016), 26.
[15] A. Mielke, T. Roubíček, *Rate-independent systems. Theory and application.*, vol. 193, New York, NY: Springer, 2015.
[16] R. Rossi, G. Savaré, *From visco-energetic to energetic and balanced viscosity solutions of rate-independent systems.*, in Solvability, regularity, and optimal control of boundary value problems for PDEs. In honour of Prof. Gianni Gilardi, Cham: Springer, 2017, 489–531.

## Anisotopic elasticity of nickel-base alloys processed by selective laser melting

Christian Krempaszky

(joint work with Thomas Obermayer, Peter Holfelder, Susanne Junghans, Ewald Werner)

Since their early days in the 1980ies the additive manufacturing techniques have been continuously developed further and now have nearly reached the stage for serial production of components. They promise a high geometric design freedom, functional integration and a high level of material utilization. Selective laser melting is an already established additive manufacturing process for small batch production of metallic components. Due to the high cooling rates and thermal gradients occurring during the process, high residual stresses are induced and the evolving microstructures as well as the resulting properties of selective laser melted alloys differ considerably from those manufactured in conventional production routes. Both strongly depends on the processing parameters. The residual stresses play a crucial role in the ability to achieve complex/slender geometries with high accuracy and may lead to in-process failure, localized deformation and component distortion during processing and during subsequent machining to final geometry, e.g. the finishing of functional surfaces or the removal of support structures. Experimental and theoretical estimation of residual stresses in selective laser melted components are challenging as the microstructures are strongly textured and result in pronounced mechanical anisotropy. Hence the knowledge of the relation between process parameters, texture and the resulting full elasticity tensor is of utmost importance for the optimization of the selective laser melting process on the base of physical based models.

Within the scope of this contribution a method is presented to determine the complete elasticity tensor of anisotropic materials via mechanical spectroscopy [1], following the basic ideas of the impulse excitation technique. It involves a sensitive microphone and electronics to record and to analyze the sound waves emitted from a free vibrating specimen by fourier analysis of the recorded acoustic signal. In the standard procedure [2], the elastic constants of isotropic elasticity are calculated by empirical analytical functions from the eigenfrequencies of the fundamental flexural and torsional modes.
An extension of this procedure to anisotropic materials is proposed as follows: A specially designed set of 15 differently oriented specimens is analyzed with respect to the eigenfrequencies of their fundamental (flexural and torsional) modes.
The identification of the components of the elasticity tensor on the basis of the set of measured eigenfrequencies represents an inverse problem, which is solved iteratively by an optimization procedure applying the Newton-Raphson method. During this procedure, the eigenfrequencies of the specimen are calculated numerically in dependence of the components of the stiffness tensor by a modal analysis using the finite element method. Since this optimization problem shows many local minima, the result of Newton-Raphson method strongly depends on the starting point.
Hence a good initial estimation of the elasticity tensor is necessary. This is realized by modifying the modulus equations from the standard [2]. The eigenfrequency of the fundamental flexural mode is used to calculate Young's modulus in longitudinal direction of each specimen, whereas the in-plane shear modulus is calculated from the eigenfrequency of the fundamental flexural mode of each of the rectangular plate-type specimens. A selection of 21 of these calculated moduli allows an initial estimation of the elasticity tensor.
The proposed approach is validated by numerical studies and allows a fast and efficient estimation of the full elasticity tensor. The method is demonstrated on a nickel-base alloy specimen set fabricated by selective laser melting. The results are compared to experimental uniaxial loading experiments and discussed with estimations of the elastic properties of the material based on single crystal constants and texture measurements performed by electron backscatter diffraction. Following the approach of Cowin [3] and Baerheim [4], a harmonic decomposition of the identified anisotropic elasticity tensor, $C_{ijkl}$, is carried out, allowing an analysis of the fourth order tensor with respect to symmetry planes. Indications for some shortcomings of the measurements are the relatively high deviatoric parts of the Voigt-tensor, $C^{\cdot\cdot j}_{ij\cdot k}$, and the dilatational modulus, $C^{\cdot\cdot\cdot k}_{ijk}$. These discrepancies are also observed by comparison to texture based estimations of the elasticity tensor and can be explained by inhomogeneities and residual stresses.
Hence, a more detailed texture analysis of the specimen set and a clarification of the influence of residual stress are essential. On this basis, an optimization of the specimen geometry and an exploitation of resonant frequencies of higher order modes will be promising steps to improve the quality of the results. Finally,

following the ideas of Weber et al. [5], an approximation of the identified elasticity tensor by fourth order tensors of given symmetry classes will further help to interprete the experimental results.

## References


[1] L.B. Magalas, *Mechanical Spectroscopy - Fundamentals*, Solid State Phenomena **89** (2003), 1–22.

[2] ASTM-E-1876-15, Standard Test Method for Dynamic Young's Modulus, Shear Modulus and Poisson's Ratio by Impulse Exitation of Vibration.

[3] S.C. Cowin, M.M. Mehrabadi, *On the Identification of Material Symmetry for Anisotropic Elastic Materials*, The Quarterly Journal of Mechanics and Applied Mathematics **40** (1987), 451–476.

[4] R. Baerheim, *Harmonic Decomposition of the Anisotropic Elasticity Tensor*, The Quarterly Journal of Mechanics and Applied Mathematics **46** (1993), 391–418.

[5] M. Weber, R. Glüge, A. Bertram, *Distance of a stiffness tetrad to the symmetry classes of linear elasticity*, International Journal of Solids and Structures **156-157** (2019), 281–293.


## Two universal laws for plastic flows

Khanh Chau Le

It is experimentally observed that a dislocated crystal deforming at constant strain rate and fixed ambient temperature will approach a steady state of plastic flow, and the corresponding steady-state flow stress, $\sigma_{\mathrm{s}}$, depends on the ambient temperature $T$ and the strain rate $\dot{\varepsilon}$. Kocks and Mecking [1] were the first to formulate the following universal law for the plastic flow of fcc-crystals: The steady-state flow stress is a function of the combination of ambient temperature and strain rate, $(T/T_{\mathrm{P}})\ln(\dot{\varepsilon}_{\mathrm{r}}/\dot{\varepsilon})$. Here $T_{\mathrm{P}}$ is an energy barrier expressed in the temperature unit, while $\dot{\varepsilon}_{\mathrm{r}}$ is a reference strain rate. However, the empirical quadratic function proposed in [1], which contains the square root of this combination, is not appropriate for two reasons: (i) this function does not fit the experimentally observed steady-state flow stresses, which are usually greater than those obtained by extrapolation based on the Voce law, (ii) it cannot be derived from the first principle calculation. The alternative scaling law for the steady-state flow stress can be obtained from the kinetics of thermally activated dislocation depinning first proposed by Langer, Bouchbinder and Lookman [2]. Applying the inverse relationship to the double exponential formula for the plastic strain rate (see Eq. (5.4) in [2]) to the steady state, the following scaling law is obtained

$$\frac{\sigma_{\mathrm{s}}}{\sigma_{\mathrm{Ts}}} = \ln\Big(\frac{1}{\frac{T}{T_{\mathrm{P}}}\ln(\frac{\dot{\varepsilon}_{\mathrm{r}}}{\dot{\varepsilon}})}\Big). \tag{1}$$

Here, $\sigma_{\mathrm{Ts}} = \mu(T)\alpha b\sqrt{\rho_{\mathrm{s}}}$ is the steady-state Taylor stress, $\mu(T)$ the shear modulus that depends on the ambient temperature, $b$ the Burgers' vector, $\rho_{\mathrm{s}}$ the steady-state dislocation density, and $\dot{\varepsilon}_{\mathrm{r}} = b\sqrt{\rho_{\mathrm{s}}}/t_0$, where $t_0$ is the time characterizing the depinning rate. It must be emphasized that (1) is derived under the assumption that the depinning rate, by being the slow "bottleneck", is dominant, and that

therefore the time for dislocations to move between pinning sites and specific effects such as cross slip could be neglected. The other main assumption is that the energy barrier and the steady-state dislocation density are independent of strain rate and temperature. The scaling law (1) provides the method for determining the three material parameters $s = \alpha b\sqrt{\rho_{\mathrm{s}}}$, $T_{\mathrm{P}}$, and $\dot{\varepsilon}_{\mathrm{r}}$ from the experimental data. To the author's knowledge, this has not yet happened, so it remains unclear whether this law is supported by the experiment and in what temperature and strain rate range it is valid. To clarify this matter I use the data obtained from the compression tests of copper (aluminum) at three (four) different elevated temperatures and four (five) different strain rates [3], with the quasi-static case being excluded, and identify that, for pure copper, $s = 6.3915 \times 10^{-3}$, $T_{\mathrm{P}} = 45000\,\mathrm{K}$, $\dot{\varepsilon}_{\mathrm{r}} = 3.16 \times 10^{12}/\mathrm{s}$, while for pure aluminum, $s = 5.4526 \times 10^{-3}$, $T_{\mathrm{P}} = 27800\,\mathrm{K}$, $\dot{\varepsilon}_{\mathrm{r}} = 7.5 \times 10^{11}/\mathrm{s}$. Note that the shear modulus depends on the ambient temperature according to $\mu(T) = \mu_1 - D/(\exp(T_1/T) - 1)$, where $\mu_1 = 51.3\,\mathrm{GPa}$, $D = 3\,\mathrm{GPa}$, $T_1 = 165\,\mathrm{K}$ for copper, and $\mu_1 = 28.8\,\mathrm{GPa}$, $D = 3.44\,\mathrm{GPa}$, $T_1 = 215\,\mathrm{K}$ for aluminum (see [4]).

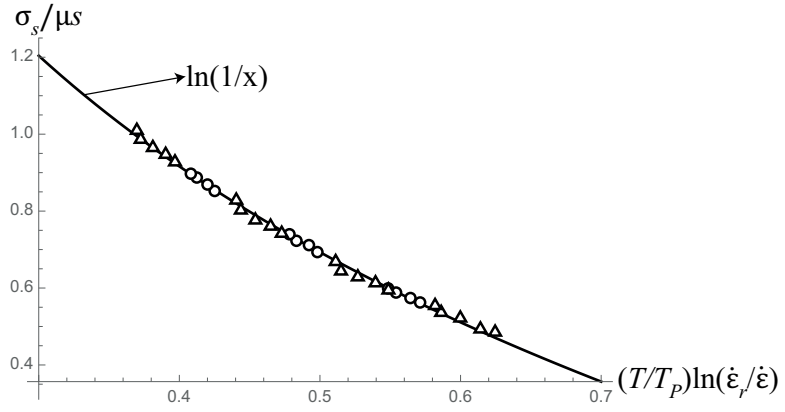


FIGURE 1. Dimensionless steady-state flow stresses $\frac{\sigma_{\mathrm{s}}}{\mu s}$ versus $\frac{T}{T_{\mathrm{P}}} \ln(\frac{\dot{\varepsilon}_{\mathrm{r}}}{\dot{\varepsilon}})$ for copper (circle) and aluminum (triangles) and the master curve $y = \ln(1/x)$.

Fig. 1 shows the data points with $x$-coordinate being $(T/T_{\mathrm{P}}) \ln(\dot{\varepsilon}_{\mathrm{r}}/\dot{\varepsilon})$ and $y$-coordinate being $\sigma_{\mathrm{s}}/\mu(T)s$ of copper (circles) and aluminum (triangles) as well as the master curve $y = \ln(1/x)$. It is seen that most points lie almost exactly on this curve. Since the experimental points of other fcc-crystals such as silver or nickel are also close to those of copper and aluminum [1], it is concluded that Eq. (1) is the validated scaling law for the steady-state flow stress of these materials for temperatures from room temperature to two-thirds of the melting temperature and for strain rates from 1/s to $10^{10}$/s.

The law (1), however, does not say anything about how the stress and dislocation density approach the steady state. This behavior can be extracted from a second

law for plastic flows formulated also by Langer et al. [2] as follows: The configurational entropy of the subsystem of dislocations must increase and reach its maximum in the steady state. This law is the consequence of the thermodynamics and statistical mechanics of configurational subsystem of moving dislocations regarded as a dissipative driven system. The underlying thermodynamics is based on the existence of slow and fast variables in this system. Fast variables are coordinates of dislocations. Slow variables are elastic deformation, dislocation density, and configurational entropy (or effective disorder temperature). The conditions under which fast variables can be averaged out are not the same as those of reversible Hamiltonian systems for which ergodicity is crucial [5]. The laws governing the slow variables are also not the same as those of equilibrium thermodynamics of ergodic Hamiltonian systems. Even the steady state, regarded as "equilibrium" state of the configurational subsystem, is not a strict equilibrium, since dislocations are permanently pinned and depinned and move between the pinning sites so that the body flows plastically at the constant strain rate. This is similar to the slow change of amplitude of non-linear vibration of a forced dissipative oscillator towards the steady-state amplitude after the fast oscillation is averaged out [6, 7]. Although the dissipative configurational subsystem of dislocations is driven, it seems physically reasonable that the configurational entropy must increase and reach a maximum in the steady state regarded as "equilibrium".

The theory based on the law of maximum configurational entropy was proposed in [2] and slightly modified in [8] for polycrystals. The problem with using system of governing equations to simulate stress-strain curves is the choice of parameters. Unfortunately, the choice made in [2] is not fully consistent with the scaling law (1). For instance, the selected value of $T_{\mathrm{P}} = 40800\,\mathrm{K}$ for copper is somewhat smaller than the value 45000 K identified from Eq. (1). Similarly, for the ad-hoc selected parameters $\chi_0$, $a$, and $t_0$, it is found that $\dot{\varepsilon}_{\mathrm{r}} = 1.35 \times 10^{11}/\mathrm{s}$ which is less than the value $3.16 \times 10^{12}/\mathrm{s}$ identified above. Therefore the inconsistent and ad-hoc choices made in [2] are abandoned and all parameters and initial conditions are identified with the large-scale least-squares analysis [10, 9]. This yields in addition to $T_{\mathrm{P}}$, $s$, and $\dot{\varepsilon}_{\mathrm{r}}$ the three basic parameters for copper $\tilde{\chi}_0 = 0.2177$, $K_\rho = 0.833$, $K_\chi = 2.66$. With this I find that $r = 0.0635$, $\tilde{t}_0 = 3.18 \times 10^{-14}\,\mathrm{s}$ which is also consistent with Eq. (1). I have simulated several stress-strain curves for copper under compression at different thermal and loading conditions and compared them with the experimental points taken from [3, 11]. The excellent agreement between theory and experiment and the consistency with the formulated universal laws allows the conclusion that this theory can be used to predict the plastic flows of fcc-crystals over a wide range of strain rates and temperatures.

## References

[1] U.F. Kocks, H. Mecking, Prog. Mater. Sci. **48** (2003), 171.
[2] J.S. Langer, E. Bouchbinder, T. Lookman, Acta Mater. **58** (2010), 3718.
[3] S.K. Samanta, J. Mech. Phys. Solids **19** (1971), 117.
[4] Y.P. Varshni, Phys. Rev. B **2** (1970), 3952.

[5] D. Ruelle, *Thermodynamic Formalism: the Mathematical Structure of Equilibrium Statistical Mechanics*, Cambridge University Press, Cambridge, 2004.
[6] J. Guckenheimer, P. Holmes, *Nonlinear Oscillations, Dynamical Systems, and Bifurcations of Vector Fields*, Springer Verlag, Berlin, 2013.
[7] K.C. Le, L.T.K. Nguyen, *Energy Methods in Dynamics*, Springer Verlag, Berlin, 2014.
[8] K.C. Le, T.H. Le, T.M. Tran, Int. J. Eng. Sci. **149** (2020), 103230.
[9] K.C. Le, T.M. Tran, Int. J. Eng. Sci. **119** (2017), 50.
[10] K.C. Le, T.M. Tran, J.S. Langer, Phys. Rev. E **96** (2017), 013004.
[11] P.S. Follansbee, U.F. Kocks, Acta Metall. **36** (1988), 81.

## Plate theories: A mixed Vekua and consistent approximation approach

Michael Meyer-Coors
(joint work with Reinhold Kienzler and Patrick Schneider)

Plates are thin, plane structures, which are typically loaded transversally to their midplanes. The classical approach to obtain plate theories invokes kinematical a-priori assumptions. Exemplarily the Kirchhoff plate theory and the Reissner-Mindlin plate theory may be mentioned. Systematic approaches, on the contrary, try to avoid a-priori assumptions. They are based on the threedimensional theory of linear ealsticity. By applying the first variation to it, equating it with zero, using integration by parts only in $x_1$ and $x_2$ direction and substituting the virtuell quantities by their taylor series, the quasi twodimensionell problem with the global Dirichlet and Neumann boundary conditions and the global equilibrium conditions is obtained. This problem can be seperated into the plate and the disc problem for at least monotropic material (with the midplane as symmetrie plane). Thus, the plate problem can be treated isolated. So far, there are infinitely many equations with infinitely many unknowns. To get to calculable equation systems, an approximation is necessary. One possiblity is the Vekua-type approximation [1]. Here, a series expansion of the displacements is applied and the corresponding truncation is done after a certain number of displacement coefficients. Another approximation method, which is also based on series expansions, is described by Kienzler & Schneider [2]. They discovered that the magnitude of each summand of the potential energy is almost completely determined by powers of a geometric factor. This approach is called the consistent approximation approach. Both methods lead to hierarchic theories, which are distinguished by their approximation order.
Based on the consistent approximation approach, a split of displacement coefficients, which is applicable for any approximation order, is carried out. The resulting scheme allows to obtain a reduction equation for every displacement coefficient of a certain order. Especially, the basic differential equations which resemble the Kirchhoff plate theory by first order approximation can be easily obtained. By applying the scheme, the original triangular-like coefficient matrix (of the PDE system) turns into a rectangular coefficient matrix, the form of Vekua-type plate theories. The evolving theory is called complete plate theory. To verify the scheme, i.e., to proof that every complete theory leads to reduction equations for every displacement coefficient, the determinants of the coefficient matrices are studied.

For complete reducibility of the equation systems, they have to be unequal to zero. Driven by the observation that the coefficent matrices of the complete plate theories have an interlaced structure (like a Matrjoschka), the problem is reduced to the calculation of a Hilbert matrix with only odd denominators. A closed formula to determine the inverse and the determinant was found so that the proof is almost finished.
For the special cases of isotropy and transverse isotropy it has been shown that the reduction equations, gained by solving the PDE systems of the complete plate theories, identically fulfill the local equilibrium conditions, the local Neumann boundary conditions and the local Dirichlet boundary conditions. To proof that all reduction equations of every order satisfy the local conditions, the global and local conditions have to be linearly interdependent. This proof is subject of ongoing research.

## References

[1] Il'ja N. Vekua, Monographs, advanced texts and surveys in pure and applied mathematics. vol. 25: Shell theory: General methods of construction. Boston: Pitman, 1985.
[2] R. Kienzler, P. Schneider, *Second-order linear plate theories: Partial differential equations, stress resultants and displacements*, International Journal of Solids and Structures **115-116** (2017), 14–26. http://dx.doi.org/10.1016/j.ijsolstr.2017.01.004.

## On finite-strain thermo-viscoelasticity

Alexander Mielke
(joint work with T. Roubíček)

In [4] we provide a mathematical existence theory for a thermodynamically consistent model for thermo-viscoelasticity at finite strain. We denote by $\Omega \subset \mathbb{R}^d$ the bounded reference configuration, by $y(t,\cdot) : \Omega \to \mathbb{R}^d$ the time-dependent deformation, and by $\theta(t,\cdot) : \Omega \to [0,\infty[$ the temperature field. Moreover, $F(t,x) = \nabla y(t,x) \in \mathbb{R}^{d\times d}$ is the deformation gradient.
There are several nontrivial challenges to be overcome:

- Even for elastostatics frame-indifference and the blow-up of the energy density $F \mapsto \varphi(F,\theta)$ for infinite volume compression, i.e. $\det F \searrow 0$, it is impossible to control the stresses that will be needed for the dynamic theory.
- We will neglect inertia to avoid formation of shocks.
- The viscous stresses need to obey time-dependent frame indifference, see [1, 8], such that the viscous dissipation only controls $\dot C = F^\top \dot F + \dot F^\top F$, but not the rate $\dot F$ of the deformation gradient $F$.
- The coupling of the temperature $\theta$ and the deformation $F$ leads to latent heat effects, thermal expansion etc. Moreover, the right-hand side of the heat equation includes the viscous heating that can only be controlled in $\mathrm{L}^1([0,T]\times\Omega)$.

To tackle these challenges we consider a second-grade material, where the stored elastic energy is enhanced with a term depending on the second gradient $\nabla^2 y$ of

the deformation. This term leads to a mathematical regularization making the deformation tensor $F = \nabla y$ Hölder continuous.
More precrisely, using a total free energy of the form

$$\mathcal{F}(y,\theta) = \int_\Omega \big\{\varphi_{\rm elast}(\nabla y) + \phi_{\rm joint}(\nabla y,\theta) + H(\nabla^2 y)\big\}\,{\rm d}x$$

we can define the total internal energy via $e(F,\theta) = \varphi_{\rm elast}(F) + \mathfrak{w}(F,\theta)$ with $\mathfrak{w}(F,\theta) = \phi_{\rm joint}(\nabla y,\theta) - \theta\,\partial_\theta\phi_{\rm joint}(\nabla y,\theta)$ and obtain

$$\mathcal{E}(y,\theta) = \int_\Omega \big\{\varphi_{\rm elast}(\nabla y) + \mathfrak{w}(\nabla y,\theta) + H(\nabla^2 y)\big\}\,{\rm d}x.$$

The viscoelastic dissipation is characterized by a dissipation potential in the form

$$\mathcal{R}(y,\theta,\dot y) = \int_\Omega \zeta(\nabla y,\theta,\ \nabla\dot y)\,{\rm d}x$$

where time-dependent frame-indifference implies that $\zeta$ has the form $\zeta(F,\theta,\dot F) = \widehat{\zeta}(C,\theta,\dot C)$ with $C = F^\top F$ and $\dot C = F^\top\dot F + \dot F^\top F$, see [1, 8].
The linear momentum equation (neglecting inertia) can be written in the abstract form $0 = {\rm D}_{\dot y}\mathcal{R}(y,\theta,\dot y) + {\rm D}_y\mathcal{F}(y,\theta)$. The heat equation is best formulated for the "thermal part" $\mathfrak{w}$ of the internal energy, namely

$$\dot{\mathfrak{w}} - {\rm div}\big(\mathbb{K}(\nabla y,\theta)\nabla\theta\big) = \partial_{\dot F}\zeta(\nabla y,\theta,\nabla\dot y){:}\nabla\dot y + \partial_F\phi_{\rm joint}(\nabla y,\theta){:}\nabla\dot y.$$

Besides of the classical assumption in this area, the following special constitutive conditions are imposed:

(1a) coercivity: $\varphi_{\rm elast}(F) \ge c({\det F})^{-\delta}$, $H(A) \ge c|A|^r - K$, $\dfrac{1}{\delta} + \dfrac{1}{r} \le \dfrac{1}{d}$,

(1b) stress control: $|\partial_F\phi_{\rm joint}(F,\theta)|^2 \le K\phi_{\rm elast}(F) + K^2$,

(1c) viscosity: $\widehat{\zeta}(C,\theta,\dot C) = \dfrac{1}{2}\dot C{:}\mathbb{D}(C,\theta){:}\dot C \ge c|\dot C|^2$,

where $c$ and $K$ are a suitable small and big constant.
The main result in [4] shows that for all initial conditions $(y(0),\theta(0)) = (y_0,\theta_0)$ with $\mathcal{E}(y_0,\theta_0) < \infty$, there exists a suitable weak solution $(y,\theta) : [0,T] \to {\rm W}^{2,r}(\Omega)\times {\rm L}^1(\Omega)$ satisfying

(2a) $y \in {\rm C}^0_{\rm w}([0,T];{\rm W}^{2,r}(\Omega)) \cap {\rm H}^1([0,T];{\rm H}^1(\Omega))$ and

(2b) $\theta \in {\rm L}^1([0,T];{\rm W}^{1,1}(\Omega)) \cap {\rm L}^q([0,T];{\rm W}^{1,q}(\Omega))$ for all $q \in [1, \frac{d+2}{d+1}[$.

Moreover, the solution is constructed to satisfy the energy balance $\mathcal{E}(y(t),\theta(t)) = \mathcal{E}(y_0,\theta_0)$ and the mechanical energy-dissipation balance

(3a) $$\mathcal{M}(y(T)) + \int_0^T \Big\{2\mathcal{R}(y,\theta,\dot y) + \int_\Omega \partial_F\phi_{\rm joint}(\nabla y,\theta){:}\nabla\dot y\,{\rm d}x\Big\}\,{\rm d}t = \mathcal{M}(y_0),$$

(3b) where $\mathcal{M}(y) = \displaystyle\int_\Omega \big\{\varphi_{\rm elast}(\nabla y) + H(\nabla^2 y)\big\}\,{\rm d}x$.

The proof of the result relies on three mathematical tools that are of independent interest:

(A) The global invertibility theory for second-grade materials pioneered by Healey and Krömer in [3] relies on the coercivity assumption (1a). Given any constant $M$ there exist positive constants $K$ and $c$ such that $y \in \mathrm{W}^{2,r}_{\mathrm{Dir}}(\Omega)$ with $\mathcal{M}(y) \leq M$ satisfies

$$\det \nabla y(x) \geq c \quad \text{and} \quad \|\nabla y\|_{\mathrm{C}^\alpha} + \|(\nabla y)^{-1}\|_{\mathrm{C}^\alpha} \leq K.$$

(B) The positive lower bound for the determinant is crucial for exploiting the second tool, which is a generalized version of Korn's inequality. The relevant version was derived by Neff and Pompe in [6, 7] and provides, via (1c), an $\mathrm{L}^2$ control of $\nabla \dot{y}$ by the viscous dissipation, viz.

$$\int_\Omega |\nabla y^\top \nabla V + \nabla V^\top \nabla y|^2 \,\mathrm{d}x \geq c_{\mathrm{Korn}}(M)\|V\|^2_{\mathrm{H}^1}$$

for all $y$ with $\mathcal{M}(y) \leq M$ and $V \in \mathrm{H}^1_0(\Omega)$.

(C) The third mathematical tool is the abstract chain rule for semi-convex functions as devised by Brézis for convex functionals in [2, Lem. 3.3] and by [5, Sec. 2.2] for general $\lambda$-convex functionals in separable Banach spaces.

The construction of solutions is done by several approximations: (i) the viscous dissipation is enhanced by an artificial and physically unacceptable dissipation $\frac{\varepsilon}{2}|\dot{F}|^2$ (cf. [1]); (ii) the viscous heating is modified to $2\zeta(\cdots)/(1+2\varepsilon\zeta(\cdots))$ which makes this right-hand side bounded; and (iii) the time is discretized with time step $\tau > 0$ to exploit incremental minimization techniques.

Because of (iii) we lose the control on the energy balance $\mathcal{E}(y^{\varepsilon,\tau}(t)) \leq \mathcal{E}(y_0, \theta_0)$, but we still obtain a discrete counterpart of mechanical energy balance (3), namely

$$\mathcal{M}(y^{\varepsilon,\tau}(T)) + \int_0^T \Big\{ \varepsilon \|\nabla \dot{y}^{\varepsilon,\tau}\|^2 - \|\partial_F \phi_{\mathrm{joint}}(\nabla y^{\varepsilon,\tau}, \theta^{\varepsilon,\tau}\|_{\mathrm{L}^2} \|\nabla \dot{y}^{\varepsilon,\tau}\|_{\mathrm{L}^2} \Big\} \,\mathrm{d}t \leq \mathcal{M}(y_0).$$

This estimate allows us to obtain $\varepsilon$-dependent a priori estimates that control the limit $(y^{\varepsilon,\tau}, \theta^{\varepsilon,\tau}) \to (y^\varepsilon, \theta^\varepsilon)$ for $\tau \searrow 0$. Next, in the time-continuous case the chain rule (C) can be employed to regain the energy inequality $\mathcal{M}(y^\varepsilon(t)) \leq \mathcal{E}(y^\varepsilon(t), \theta^\varepsilon(t)) \leq \mathcal{E}(y_0, \theta_0)$.

With this, the invertibility theory (A) and the generalized Korn inequality (B) can be applied on the sublevel $\big\{ y \in \mathrm{W}^{2,r}(\Omega) \,\big|\, \mathcal{M}(y) \leq \mathcal{M}(y_0) \big\}$, uniformly in $\varepsilon > 0$. Thus, the limit $\varepsilon \searrow 0$ can be performed as well with the weak convergence $\nabla \dot{y}^\varepsilon \rightharpoonup \nabla \dot{y}$ in $\mathrm{L}^2([0,T]\times\Omega; \mathbb{R}^{d\times d})$. To pass to the limit in the heat equation with the right-hand side $2\zeta(\nabla y^\varepsilon, \theta^\varepsilon, \nabla \dot{y}^\varepsilon)/(1+2\varepsilon\zeta(\cdots))$ that is only bounded in $\mathrm{L}^1([0,T]\times\Omega)$, we exploit the abstract chain rule (C) for $\mathcal{M}$ and improve the weak convergence of $\nabla \dot{y}^\varepsilon$ to strong convergence.

*Acknowledgments.* The research was partially supported by Deutsche Forschungsgemeinschaft (DFG) through grant CRC 1114 "*Scaling Cascades in Complex Systems*" (Project Number 235221301), Subproject B01 *Fault networks and scaling properties of deformation accumulation.*

## References

[1] S. S. Antman, *Physically unacceptable viscous stresses*, Z. Angew. Math. Phys. **49**(6) (1998), 980–988.

[2] H. Brézis, *Opérateurs maximaux monotones et semi-groupes de contractions dans les espaces de Hilbert*, North-Holland Publishing Co., Amsterdam, 1973.

[3] T. J. Healey, S. Krömer, *Injective weak solutions in second-gradient nonlinear elasticity*, ESAIM Control Optim. Calc. Var. **15** (2009), 863–871.

[4] A. Mielke, T. Roubíček, *Thermoviscoelasticity in Kelvin-Voigt rheology at large strains*, To appear in Arch. Rational Mech. Anal. WIAS preprint 2584 (2019).

[5] A. Mielke, R. Rossi, G. Savaré, *Nonsmooth analysis of doubly nonlinear evolution equations*, Calc. Var. Part. Diff. Eqns. **46**(1-2) (2013), 253–310.

[6] P. Neff, *On Korn's first inequality with non-constant coefficients*, Proc. Roy. Soc. Edinburgh Sect. A **132** (2002), 221–243.

[7] W. Pompe, *Korn's first inequality with variable coefficients and its generalization*, Comment. Math. Univ. Carolinae **44**(1) (2003), 57–70.

[8] B. Svendsen, A. Bertram, *On frame-indifference and form-invariance in constitutive theory*, Acta Mechanica **132** (1999), 195–207.


## Making, testing, and modeling of pantographic structures


Wolfgang H. Müller

(joint work with Gregor Ganzosch)


In the recent past the fabrication of complex-designed and function-oriented structures became possible due to new developments in the additive manufacturing and prototyping industries. This progressive manufacture technique enables the combination of specially tailored (sub)structures with custom designed materials resulting in a new class of material, the so called meta-materials.

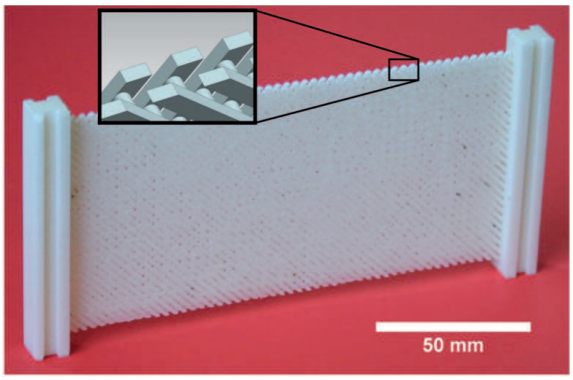


Figure 1. Pantographic structure developed by [2] and manufactured at the Institute of Mechanics at Technische Universität Berlin by means of an FDM technique (using polylactide as raw powder on an Ultimaker 3 extended printer).

Meta-materials are able to show an extraordinary deformation behavior on the macroscopic scale, which is strongly dependent on the substructure in microscopic scale. Pantographic Structures (PS), which can be described as meta-materials with a substructure composed of two orthogonal arrays of beams, connected by internal cylinders (see Fig. 1), were manufactured by using three different additive

manufacturing techniques - Fused Deposition Modeling (FDM), Direct Melting Laser Sintering (DMLS), and Selective Laser Sintering (SLS). In general, effective properties are carefully chosen by designing microscopic constituents in the substructure in order to achieve specially desired properties ([1, 2, 3]). Therefore the mechanical performance of PSs depends not only on the global structure, but also on the morphology of their subunits consisting of so-called inner parameters, which are repeated periodically in the substructure.

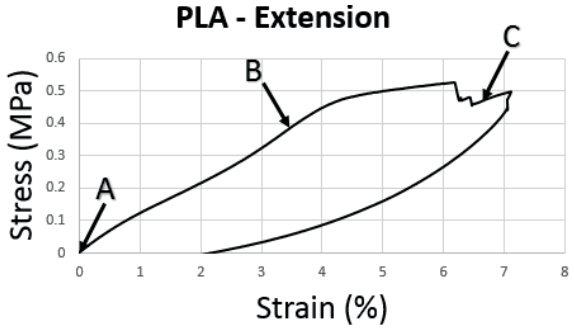


FIGURE 2. Stress-Strain diagram of an extension test of PS made out of polyactide (PLA). Points A, B, and C, correspond to the different loading steps from Fig. 3.

Samples with different inner parameters have been tested in standard extension and shear tests (Tytron MTS 250, Minnesota, USA), as well as in torsion tests (Zwick Z010, Ulm, Germany). Different materials were chosen: Polyamide (PA), Polylactide (PLA), and Aluminum (ALU). Digital Image Correlation (DIC) was used to determine displacements and strains on the specimen surfaces by means of a standard digital single-lens reflex camera Canon 600D (Canon Inc., Tokyo, Japan) and the open-source GOM Correlation software (GOM GmbH, Braunschweig, Germany).

Loaded specimen respond linear elastically with a strong resilient deformation behavior being capable to resist even higher loads after internal failure. Results from a discrete 2D-model of the Hencky type (for further informations see [4]) was compared with experimental results of extension- and shear-tests in the elastic range because of model limitations.

In Fig. 2 the stress-strain diagram of FDM-printed PS (PLA) is shown. Linear elastic deformation can be recognized up to an enlargement of about $\varepsilon = 3.5$ % (corresponding to Fig. 3B). Resilient response occurs at about $\varepsilon = 6.5$ % (corresponding to Fig. 3C). Because of the laterally asymmetrical structure of PS, non symmetric deformation was measured during extension tests (see DIC in Fig. 3). Therefore [5] introduced an extended version of the PS by changing the inner parameters resulting in so-called Bi-Pantographic Structures (Bi-PS, see Fig. 4). Being axially loaded in an extension test Bi-PS deform symmetrically in contrast to PS. Another very promising advantage of this kind of structure lies in the very large elastic deformation behavior. Bi-PS are capable to resist outer axial loads (extension) up to about 40 percent of elongation (displacement of 80 mm) in the non-linear elastic regime (Fig. 5A). This exceptional response was also calculated with the help of an in-plane discrete model (see Fig. 5A; right hand side). Here, the rotational stiffness of the pivot and flexural stiffness of the beam mark the inner parameters of the substructure, which had been determined in experiments.

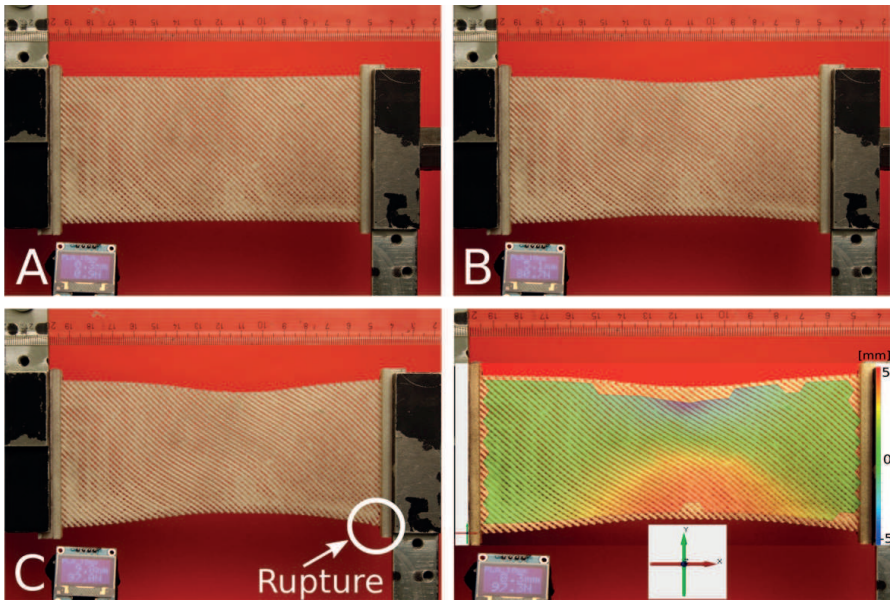


FIGURE 3. Image sequence of PS during tensile loading. Step A - C correspond to the the marked points in Fig. 2. The picture in the lower right corner shows exemplary the calculated necking in $y$-direction by means of 2D-DIC shortly before first rupture occurs.

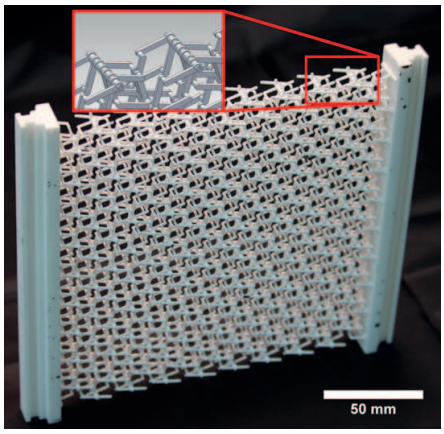


FIGURE 4. Quadratic Bi-Pantographic structure developed by [5] printed on a Formiga P 100 using SLS technique.

Furthermore, in a shear test the linear elastic response was calculated resulting in an elongation in shear-direction of about 20 percent (shear-displacement of about 30 mm). These results are in good agreement with the experimental measurements (Fig. 5B).
It should also be mentioned that two different DMLS-printed PS have been investigated in torsion tests as well. The heat-treated as well as the non-heat-treated specimen show small elastic deformations. Further analysis would go beyond the scope of this discussion but are available in [6].

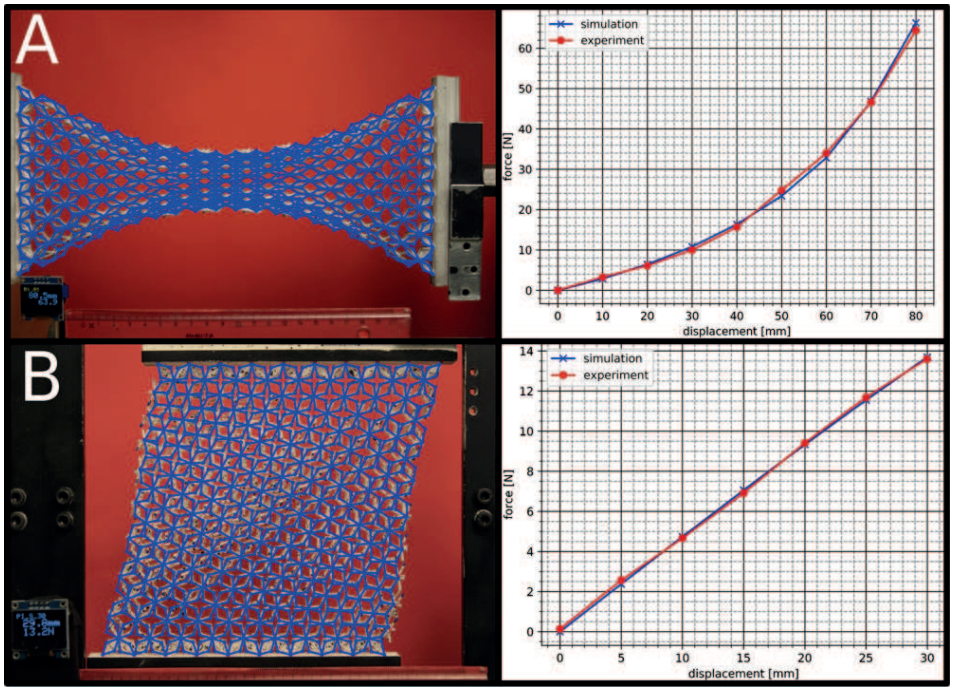


FIGURE 5. A: Overlay of a discrete model (blue) on a rectangular specimen Bi-PS during an extension experiment with about 40 percent of axial elongation. B: Overlay of a discrete model (blue) on a quadratic specimen Bi-PS during a shearing experiment with about 30 percent of axial elongation.

## REFERENCES

[1] L. J. Gibson, M. F. Ashby, *Cellular solids: structure and properties*, Cambridge University Press, 1999.

[2] F. dell'Isola, T. Lekszycki, M. Pawlikowski, R. Grygoruk, L. Greco, *Designing a light fabric metamaterial being highly macroscopically tough under directional extension: First experimental evidence*, Zeitschrift für angewandte Mathematik und Physik **66**(6) (2015), 3473–3498.

[3] E. Barchiesi, M. Spagnuolo, L. Placidi, *Mechanical metamaterials: a state of the art*, Mathematics and Mechanics of Solids **24**(1) (2019), 212–234.

[4] E. Turco, F. dell'Isola, N L. Rizzi, R. Grygoruk, W. H. Müller, C. Liebold, *Fiber rupture in sheared planar pantographic sheets: Numerical and experimental evidence*, Mechanics Research Communications **76** (2016), 86–90.

[5] E. Barchiesi, S. Eugster, F. dell'Isola, F. Hild, *Large in-plane elastic deformations of bi-pantographic fabrics: asymptotic homogenization and experimental validation*, Mathematics and Mechanics of Solids (2020), https://doi.org/10.1177/1081286519891228.

[6] G. Ganzosch, K. Hoschke, T. Lekszycki, I. Giorgio, E. Turco, W. H. Müller, *3D-Measurements of 3D-Deformations of Pantographic Structures*, Technische Mechanik **38**(3) (2018), 233–245.

## Breaking the limits of metal strength

Eugen Rabkin

We studied the uniaxial compression behavior of micro- and nanoparticles of several elemental metals (Au [1], Ni [2], Ag [3], Mo) and alloys (Ni-Fe, Ni-Co, Au-Ag). The particles were obtained by solid state dewetting of thin metal films and multilayers deposited on sapphire substrates. The high homological temperatures employed in dewetting process ensure the low concentration of dislocations and their sources in the particles. The particles compressed with a flat diamond punch exhibit purely elastic behavior up to very high values of strain approaching 10 %, followed by a catastrophic plastic collapse. The uniaxial yield strength of the particles defined as an engineering stress at the point of catastrophic collapse reached the astonishing values of 34 GPa and 46 GPa for the smallest faceted particles of Ni and Mo, respectively. The atomistic molecular dynamic simulations of the particles compression demonstrated that the catastrophic plastic yielding of the particles is associated with the multiple nucleation of dislocations at the facet corners or inside the particles. The latter, homogeneous nucleation mode resulted in higher particle strength. The size effect in compression was observed both in the experiments and in atomistic simulations, with smaller particles exhibiting higher compressive strength. We discussed the stronger size effect observed in the experiment (as compared with simulations) in terms of the effect of residual defects trapped in the particles [4]. Finally, we produced Au-Ag core-shell nanoparticles by coating the single crystalline Ag nanoparticles with a polycrystalline Au shell. The core-shell nanoparticles exhibited much lower strength than their single crystalline pure Ag counterparts. We related this decrease in strength with the activity of grain boundaries in the polycrystalline Au shell.

An ultrahigh strength of metal nanoparticles observed in the experiments indicates that the contribution of diffusion-controlled Cobble-like creep to the overall plastic strain increases with decreasing the particle size. We analyzed the experiment on in-situ pseudo-elastic deformation of Ag nanoparticles inside the transmission electron microscope [5] in terms of Ag self-diffusion along the particle-punch interface, and on the side surfaces of the particle [3]. We have considered an axisymmetric Ag particle attached to a rigid inert substrate, and compressed by a flat inert punch (Figure 1a). An irreversible change of stress-free particle height is only possible due to the self-diffusion of Ag atoms along the particle-substrate and particle-punch interfaces (Figure 1a). The Ag atoms emerging from the two interfaces are re-distributed along the side surface of the particle. The mass conservation condition requires

$$J_{c1} = J_{s1} \qquad \text{and} \qquad J_{c2} = -J_{s2} \tag{1}$$

where $J_c$ and $J_s$ are interface and surface diffusion flows, respectively, at the triple line where the interface, the substrate surface, and the particle side surface meet ($r = Rc$). The indexes "1" and "2" refer to the particle-substrate and particle-punch interfaces, respectively. In what follows we will consider both interfaces in a similar way and omit the indexes "1" and "2". The evolution of side surface

topography is described by Mullins equation. The driving force for diffusion along the interfaces is the gradient of chemical potential of Ag atoms, $\mu$, at the interface:

$$J(r) = -B_{\mathrm{i}} 2\pi r \frac{\partial \mu}{\partial r} \tag{2}$$

where $J(r)$ is the total diffusion flow of Ag atoms through the circle of radius $r$ at the interface, and $B_{\mathrm{i}}$ is the interfacial Mullins coefficient:

$$B_{\mathrm{i}} = \frac{D_{\mathrm{i}} \nu_{\mathrm{i}}}{kT}. \tag{3}$$

In the expression (3), $D_{\mathrm{i}}$, and $\nu_{\mathrm{i}}$ are the self-diffusion coefficient of Ag atoms along the interface and the number of mobile atoms per unit area of the interface, respectively. $kT$ has its usual thermodynamic meaning. The condition of the rigidity of the substrate and the punch requires that the materials accretion/depletion at the interface is homogeneous, or, in other words, that the divergence of the interface

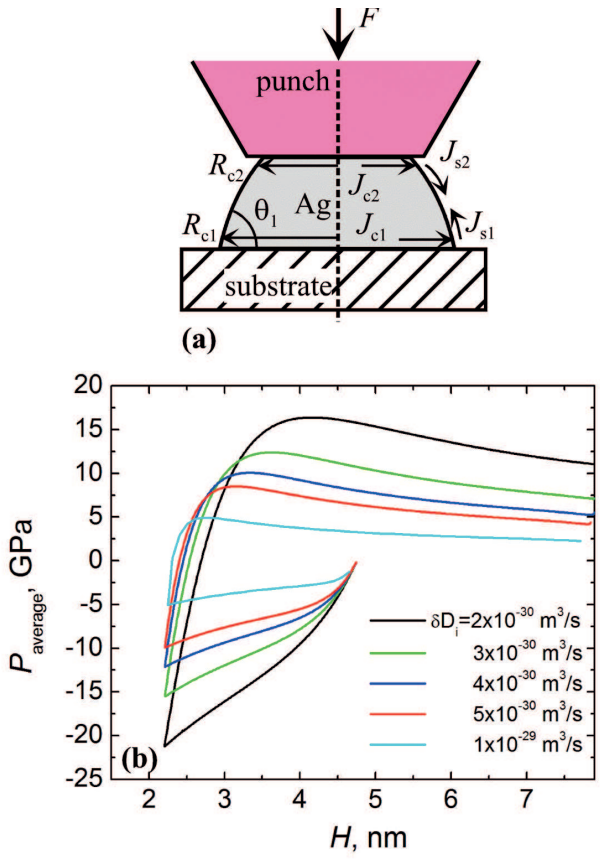


FIGURE 1. a) Schematic presentation of the diffusion model of a creep-like deformation of Ag nanoparticles controlled by Ag self-diffusion along the Ag-substrate and Ag-punch interfaces. b) The simulated dependencies of the average contact pressure, $P_{\mathrm{average}}$, on particle height, $H$, for several different values of the interface diffusivity.

diffusion flow is constant:

$$r^{-1}\frac{\partial J}{\partial r} = \text{const} = -2\pi B_{\text{i}} a \tag{4}$$

where $a$ =const. The axisymmetrical geometry of the problem requires $J = 0$ for $r = 0$ and, hence,

$$J(r) = -\pi B_{\text{i}} a r^2 \tag{5}$$

Combining equations (2) and (5) yields the following expression for the interface chemical potential:

$$\mu(r) = \mu_c + 0.25a\left(r^2 - R_{\text{c}}^2\right) \tag{6}$$

where $\mu_c = \mu(R_{\text{c}})$. The constant $a$ in equation (6) can be found by adding a uniform layer of Ag of a thickness $\mathrm{d}z$ to the interface, calculating the total change of the energy of all surfaces and interfaces in the system, and the work done against the applied load, $F$, and equating them to the total energy contribution of all Ag atoms in the added material:

$$2\pi R_{\text{c}}\Delta\gamma - F = \frac{1}{\Omega}\int_0^{R_{\text{c}}} \mu(r) 2\pi r \,\mathrm{d}r \tag{7}$$

where $\Omega$ is the atomic volume of Ag and

$$\Delta\gamma = \frac{\gamma + (\gamma_{\text{i}} - \gamma_{\text{s}})\cos\theta}{\sin\theta} \tag{8}$$

with $\gamma$, $\gamma_{\text{i}}$, $\gamma_{\text{s}}$ and $\theta$ being the surface energy of Ag, the interface energy, the surface energy of the substrate, and the contact angle of solid Ag on the substrate, respectively. Substituting equation (6) into (7) yields the value of interface diffusion flow at the triple line:

$$J(R_{\text{c}}) = J_c = 8\pi B_{\text{i}}\left(\mu_{\text{c}} - \frac{2\Delta\gamma\Omega}{R_{\text{c}}} + \frac{F\Omega}{\pi R_{\text{c}}^2}\right) \tag{9}$$

The condition of flux continuity requires matching of the interface diffusion flow given by equation (9) with the respective surface diffusion flow at the triple line. Also, the continuity of the chemical potential requires $\mu_{\text{c}} = \gamma K$, where $K$ is the curvature of the surface near the triple line. Equation (9), together with the Mullins equation for surface diffusion fully determine the evolution of the particle shape controlled by diffusion under applied load $F$. The way to treat the particle deformation under the condition of constant deformation rate is given in Ref. [3]. The results of simulation for the constant punch displacement rate of $H = 0.1$ nm/s are shown in Figure 1b for the different values of interface diffusivities $\delta D_{\text{i}}$ and the maximum compressive displacement equal to one-half of initial particle height. One can see from Figure 1b that for the room temperature interface diffusivity of $\delta D_{\text{i}} = 5.0 \times 10^{-30}\,\text{m}^3/\text{s}$ the maximum compressive stress reached in simulations is about 9.5 GPa, close to the experimentally determined strength of 8 GPa. Thus, this value of interface diffusivity can be considered as a lower bound for the actual diffusivity enabling pseudoelastic deformation of Ag nanoparticles without activating of dislocation plasticity. In conclusion, our results confirm a

transition from the dislocation-nucleation controlled plasticity to the Coble-type creep deformation with decreasing particle size.

## References


[1] D. Mordehai, S. W. Lee, B. Backes, D. J. Srolovitz, W. D. Nix, E. Rabkin, *Size effect in compression of single-crystal gold microparticles*, Acta mater. **59** (2011), 5202–5215.

[2] A. Sharma, J. Hickman, N. Gazit, E. Rabkin, Y. Mishin, *Nickel nanoparticles set a new record of strength*, Nature Communications **9** (2018), 4102.

[3] A. Sharma, N. Gazit, E. Rabkin, Y. Mishin, *Pseudoelasticity of metal nanoparticles is caused by their ultra-high strength*, Advanced Functional Materials **29** (2019), 1807554.

[4] T. J. Flanagan, O. Kovalenko, E. Rabkin, S.-W. Lee, *The effect of defects on strength of gold microparticles*, Scripta mater. **171** (2019), 83–86.

[5] J. Sun, L. He, Y.-C. Lo, T. Xu, H. Bi, L. Sun, Z. Zhang, S. X. Mao, J. Li, *Liquid-like pseudoelasticity of sub-10-nm crystalline silver particles*, Nat. Mater. **13** (2014), 1007.


## (Re-) formulation of dislocation density based crystal plasticity models in view of insights from parameter determination


Franz Roters

(joint work with Martin Diehl, Karo Sedighiani)


Dislocation density-based crystal plasticity formulations incorporate metal physics into continuum models of plastic deformation. Typically, the Orowan equation is used to relate the plastic shear rates on system $\alpha$ to the motion of dislocations through an average dislocation velocity:

$$\dot{\gamma}^\alpha = \rho^\alpha b v^\alpha, \tag{1}$$

with $\rho^\alpha$ the mobile dislocation density, $b$ the Burgers vector, and $v^\alpha$ the mean dislocation velocity. According to Kocks [1] the velocity can be calculated as:

$$v^\alpha = l_\mathrm{s}\omega_0 \exp\left[-\frac{\Delta F}{k_\mathrm{B}T}\left\{1-\left[\frac{\tau_\mathrm{T}^{*\alpha}}{\tau_0^*}\right]^p\right\}^q\right]\mathrm{sign}\left(\tau^\alpha\right), \tag{2}$$

with $l_\mathrm{s}$ the inter obstacle spacing, and $\omega_0$ the attack frequency. If the waiting time in front of obstacles is the rate limiting factor for the dislocation movement (see figure 1), the average dislocation velocity is determined by the probability of a successful jump from one obstacle to the next. At finite temperatures, thermal energy helps a dislocation to overcome a barrier by thermal activation, a process typically described by the Arrhenius-like formulation, i.e. the exponential term with $\Delta F$ the total activation energy, $k_\mathrm{B}$ the Boltzmann constant, $T$ the temperature, $\tau_\mathrm{T}^{*\alpha}$ the driving stress, and $\tau_0^*$ the critical stress to overcome the obstacle without any thermal activation, i.e. at $T = 0K$. Finally the sign of the resolved stress $\tau^\alpha$ determines the direction of shear. The athermal part of the obstacles $\tau_\mathrm{G}^\alpha$, i.e. the barrier that is too strong for thermal activation to be significant and needed to be overcome by the resolved shear stress only, can be computed from

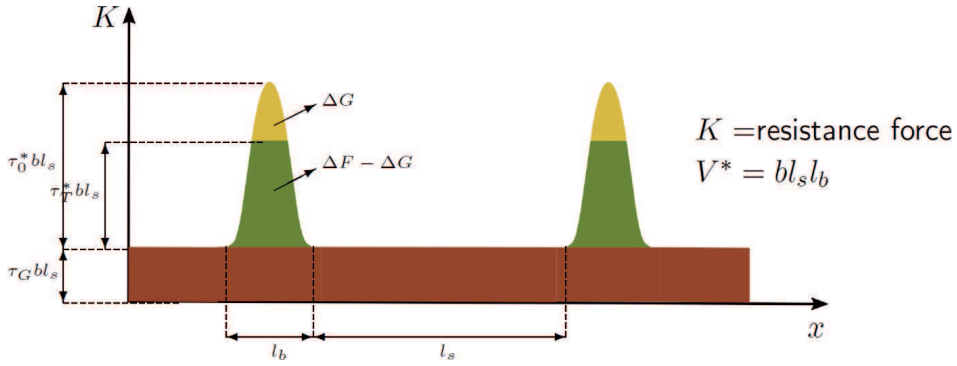


FIGURE 1. Schematic of dislocation motion in an obstacle field.

the dislocation density with a generalized Taylor law, so that the driving stress can be calculated as:

$$\tau_{\mathrm{T}}^{*\alpha} = |\tau^{\alpha}| - \mu b \left( \sum_{\alpha'=1}^{N_{\mathrm{s}}} \xi_{\alpha\alpha'} \left( \rho^{\alpha'} + \rho_{\mathrm{D}}^{\alpha'} \right) \right)^{\frac{1}{2}}, \tag{3}$$

with $\mu$ the shear modulus, $\xi_{\alpha\alpha'}$ the slip interaction coefficients, and $\rho_{\mathrm{D}}^{\alpha'}$ the dipole density. Kocks–Mecking like expressions finally provide the means to determine the dislocation density evolution.

Including all these mechanisms into a crystal plasticity formulation results in a large number of adjustable material parameters. While the upper and lower bounds for many parameters of these physics-based expressions are known, the precise determination of their values for a specific material is a time-consuming process. Even though simulations at smaller scales enable the determination of parameters such as interaction coefficients (by means of discrete dislocation dynamics), experimental data is often indispensable.

Due to the high computational effort and the many local minima we employed an efficient optimization scheme combining a genetic algorithm with the response surface methodology [2] to fit the stress–strain curves of an interstitial free steel for a wide range of temperatures and strain rates. Still we were not able to find a parameter set correctly describing the yield stress over the full temperature range, figure 2.

This raises the question, whether the parameter set found was not good enough or whether the model description is insufficient to describe the yield stress drop at high temperatures. To check the quality of the parameter optimization we used pre-calculated stress–strain curves as input, i.e. a set of curves for which a unique parameter set exists. It turned out that, while most parameters were well recovered, there was significant scatter for the parameters $\Delta F$, $p$, and $q$, when multiple fitting runs were carried out. This finding indicates a possible over-parametrization of the model suggested by Kocks [1]. This assumption is also supported by figure 3, which shows that completely different choices of the three parameters can result in a temperature dependence of $\tau^*$, which is almost identical in a large temperature range. Only for very low temperatures distinct

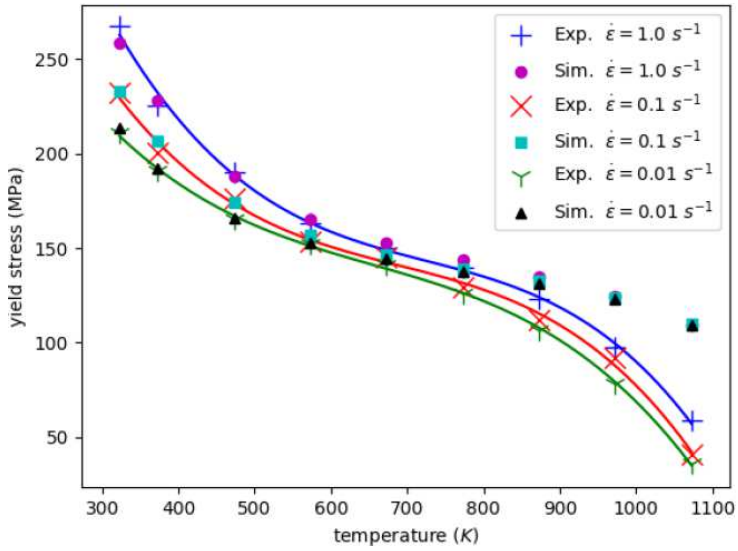


FIGURE 2. Temperature dependence of the yield stress: experiment vs. simulation.

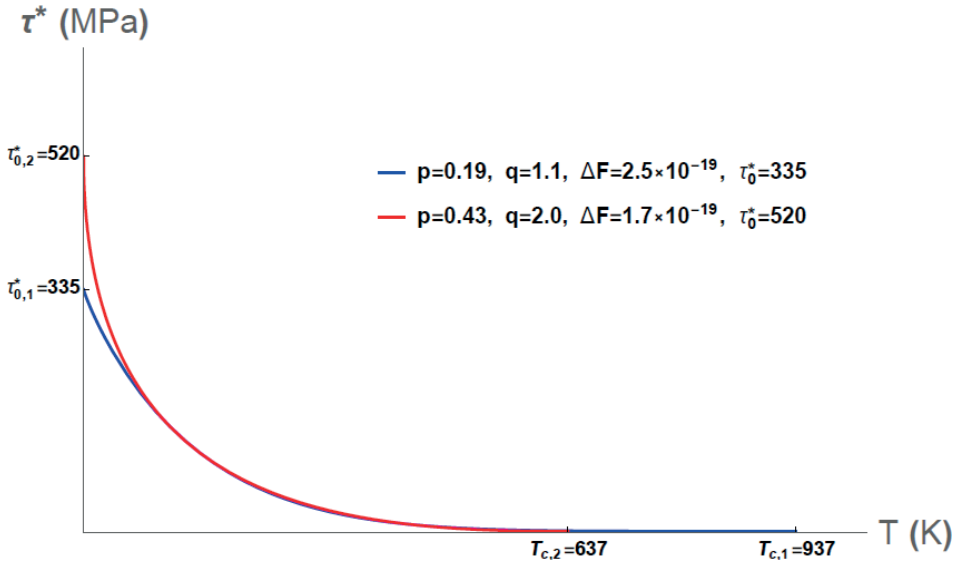


FIGURE 3. Temperature dependence of $\tau^*$ for two different parameter sets of $\Delta F$, $p$ and $q$.

differences exist, however, usually we are lacking experimental data at these low temperatures.
An alternative formulation frequently found in literature uses an activation Volume $V^*$ for the mechanical contribution to the activation energy:

$$\exp\left[-\frac{\Delta F - \tau_{\mathrm{T}}^* V^*}{k_{\mathrm{B}} T}\right]. \tag{4}$$

As can be easily shown:

$$\Delta F - \tau_{\mathrm{T}}^* V^* = \Delta F \left\{ 1 - \frac{\tau_{\mathrm{T}}^* V^*}{\Delta F} \right\} = \Delta F \left\{ 1 - \frac{\tau_{\mathrm{T}}^* V^*}{\tau_0^* V^*} \right\} = \Delta F \left\{ 1 - \frac{\tau_{\mathrm{T}}^*}{\tau_0^*} \right\}, \tag{5}$$

this formulation is almost identical to the one by Kocks, however, without the parameters $p$ and $q$. Therefore, this alternative formulation might help to overcome the problems during parameter fitting, as it reduces the number of free parameters. In addition, strain rate jump tests can help to better identify the parameters. While this might solve the issue of over-parametrization it cannot explain the yield stress drop at high temperatures. Resolving this will require additional changes in the model.

## References


[1] U. F. Kocks, A. S. Argon, M. F. Ashby, *Thermodynamics and kinetics of slip*, Pergamon Press, 1975.

[2] K. Sedighiani, M. Diehl, K. Traka, F. Roters, J. Sietsma, D. Raabe, *An efficient and robust approach to determine constitutive parameters of crystal plasticity constitutive laws from macro-scale stress-strain curves*, submitted to International Journal of Plasticity.


### About a mathematical difficulty in magnetoviscoelasticity

Anja Schlömerkemper

The mathematical analysis of the coupled system of partial differential equations in (1), which models the flow of magnetoviscoelastic materials, requires several assumptions on the elastic stored energy $W$. The aim of this talk is to discuss these assumptions from the mathematical and mechanical point of view and to indicate potential improvements. The system (1) under consideration allows for micromagnetism, finite elasticity, viscosity and dynamics. It is phrased in Eulerian coordinates and was derived in an energetic variational approach, cf. [1]. The system includes the incompressible Navier-Stokes equations, an evolution equation for the deformation tensor (transformed to Eulerian coordinates), and the Landau-Lifshitz-Gilbert equation for the magnetization vector.
For $T > 0$ and $\Omega \subset \mathbb{R}^d$ being a bounded domain with $d = 2, 3$, the system reads

$$\begin{aligned}
\partial_t v + v \cdot \nabla v - \nu \Delta v + \nabla p &= \operatorname{div}\left( W'(F) F^\top - (\nabla M)^\top \nabla M \right) + (\nabla H_{\mathrm{ext}})^\top M, \\
\operatorname{div} v &= 0, \\
\partial_t F + v \cdot \nabla F - \nabla v F &= 0, \\
\partial_t M + (v \cdot \nabla) M &= -M \times (\Delta M + H_{\mathrm{ext}}) + \Delta M + |\nabla M|^2 M \\
&\quad - (M \cdot H_{\mathrm{ext}}) M + H_{\mathrm{ext}},
\end{aligned} \tag{1}$$

where $v : (0,T) \times \Omega \to \mathbb{R}^d$ denotes the velocity field, $p : (0,T) \times \Omega \to \mathbb{R}$ is the pressure of the system, $F : (0,T) \times \Omega \to \mathbb{R}^{d \times d}$ is the deformation tensor in the Eulerian setting and $M : (0,T) \times \Omega \to \mathbb{R}^3$ the magnetization. The elastic energy density is denoted by $W : \mathbb{R}^{d \times d} \to [0, +\infty)$. The deformation tensor and the

magnetization vector satisfy the constraints $\mathrm{div} F = 0$, $|M|^2 = 1$ on $\Omega \times (0,T)$. The system is supplemented with initial and boundary conditions and obeys an energy law.

Existence of weak solutions is known globally in time for suitably small initial data if $d = 2$ and if the transport equation for $F$, equation $(1)_3$, is replaced by

$$\partial_t F + v \cdot \nabla F - \nabla v F = \kappa \Delta F$$

for some $\kappa > 0$ [1, 3]. Existence of strong solutions to the system with the regularized transport equation was shown in [3].

Existence of dissipative solutions to system (1) (without the regularization) is known globally in time and for general initial data in $d = 2, 3$ dimensions [2]. For references regarding existence of solutions for initial data that are close to equilibrium or locally in time, see the introduction of [2].

In this talk I discuss the assumptions on the elastic stored energy density $W : \mathbb{R}^{d\times d} \to [0,\infty)$ from a mathematical and mechanical perspective, respectively. As usual in continuum mechanics, $W$ is assumed to be frame-indifferent, i.e., $W(RF) = W(F)$ for all $R \in SO(d)$ and all $F \in \mathbb{R}^{d\times d}$. In the mathematical proofs, which are based on a Galerkin approach, we make use of a lower semicontinuity property of the energy functional and of $W''(F) \geq 0$. We assume the elastic stored energy density to be (i) a strictly convex $C^2$-function in [1], (ii) a convex $C^2$-function in [3] and (iii) a quadratic function, e.g., $W(F) = \frac{1}{2}|F|^2$ in [2]. In (i) and (ii) we furthermore require that there exists a $C > 0$ such that $C(|F|^2 - 1) \leq W(F) \leq C(|F|^2 + 1)$ for all $F \in \mathbb{R}^{d\times d}$.

As is well-known in continuum mechanics, the drawback of the convexity assumptions is that the energy density will not become infinite in complete compression, and self-interpenetration of matter would be possible. However, in the incompressible setting with $\det F = 1$, there is no interpenetration of matter anyhow and the convexity assumption seems not to be too bad. In the case of the regularized transport equation, i.e., in the case with $\kappa > 0$, the initial incompressibility condition $\det F_0 = 1$ is not preserved. It would be desirable to have a term penalizing deviations from $\det F = 1$, which would be non-convex. This motivates to apply the notions of polyconvexity and gradient polyconvexity in this context, which I addressed in this talk.

## References

[1] B. Benešová, J. Forster, C. Liu, A. Schlömerkemper, *Existence of weak solutions to an evolutionary model for magnetoelasticity*, SIAM J. Math. Anal. **50** (2018), 1200–1236.

[2] M. Kalousek, A. Schlömerkemper, *Dissipative solutions to a system for the flow of magnetoviscoelastic materials*, arXiv:1910.12751.

[3] M. Kalousek, J. Kortum, A. Schlömerkemper, *Mathematical analysis of weak and strong solutions to an evolutionary model for magnetoviscoelasticity*, accepted for publication in Discr. Cont. Dyn. Sys. S, arXiv:1904.07179.

### Magneto-electric composites: An algorithmic scale-bridging approach

Jörg Schröder
(joint work with Matthias Labusch)

Materials which combine two or more ferroic characteristics are known as multiferroics and can exhibit an interaction between magnetic and electric fields. This magneto-electric (ME) coupling can find applications in sensor technology or in electric field controlled magnetic data storage devices. Since ME-single-phase materials show an ME-interaction far below room temperature, the design of two-phase composites consisting of a ferroelectric matrix and magnetostrictive inclusions becomes important.
We distinguish between the direct and converse ME effect. The direct effect characterizes magnetically induced polarization, where an applied magnetic field yields a deformation of the magnetic active phase which is transferred to the electric phase. The converse effect characterizes an electrically activated magnetization.
In this contribution we discuss the two-scale modeling of micro-heterogeneous composites, which exhibit as a product property an effective (macroscopic) ME-coupling. In order to determine the effective properties, a homogenization approach – the $FE^2$-method – is designed for this multiphysics application. This connects via scale-bridging the microscopic and nanoscopic levels. To predict a realistic coupling behavior we imlemented suitable material models for the individual phases on the microscopic level which reflect the typical hysteresis curves.

### Mechanics of Biomaterials

Vadim V. Silberschmidt

Our understanding of mechanics of biological tissues, their properties and performance as well as their interaction with biomedical devices still remains limited. This is a result of multiple factors, most important being a hierarchical and heterogeneous nature of biological tissues, non-trivial loading and environmental conditions, to which they are exposed as well as multi-disciplinary nature of the processes involved. This abstract presents an overview of the latest research activities and achievements in the area of mechanics of biomaterials at Loughborough University, UK. It covers various types of biological materials and tissues – both hard (bones) and soft (muscles, etc.) – that have been studied in previous studies [1, 2, 3, 4] at various spatial and temporal domains. These studies laid a foundation for development and implementation of advanced computational modelling of mechanics of these biological tissues at different stages (healthy, diseased and traumatic conditions) and for several areas of biomedical applications (injury prevention, wound care and rehabilitation). Performed numerical simulations, on the one hand, elucidate processes of deformation of biological tissues and, on the other hand, provide solutions for design and optimization of medical and rehabilitation procedures and devices. Research on mechanical behaviour of a naturally occurring composite material, cortical bone tissue, has attracted increasing attention

over the past few decades, not only because bones play an important role in structural integrity of a musculoskeletal system, but also due to our growing knowledge of their intrinsic hierarchical structure and heterogeneous mechanical properties. This mineralized biological tissue is a main load-bearing component. Being a living tissue, cortical bone also has the ability to adapt (both its shape and internal structure) to mechanical environment through processes called remodelling. Macroscopically, the deformation mechanisms of bones differ from those of engineering materials since bones consist of a living tissue with a continuously evolving hierarchical microstructure. Mechanical properties of cortical bone vary not only from bone to bone; they demonstrate spatial viability even within the same bone due to changes of the underlying microstructure [1, 2]. Considering the wide spectrum of material properties of cortical bone and its intricate deformation processes associated with various loading modes and orientations, an investigation was performed to elucidate the effect of variations in material properties in relation to the local regions and underpinning microstructural constituents on crack propagation. The contributions of main bone's micro-constituents – osteons, Haversian canals and cement line – on evolution of crack propagation were assessed. Microscopically, the intrinsic micro-architecture of cortical bone has a significant effect on its macroscopic mechanical and fracture properties. Anisotropic deformation and fracture behaviours observed at macroscopic level are largely attributed to the preferential alignments of micro-constituents at subsequent length-scales: micro-scale for osteons and Haversian canals, or nano-scale for collagen fibrils and mineral crystals. From a fracture-toughness perspective, intricate structural hierarchy and material heterogeneity observed in the cortical bone tissue can often lead to an improved fracture resistance thanks to various fracture-toughening mechanisms. A process of deterioration of human cortical bone due to age and/or disease (e.g. osteoporosis) could increase a risk of bone fracture. Hence, the methods to predict such development and to protect patients are becoming an increasingly attractive research topic. A traditional evaluation method was to measure bone mineral density, but this single factor is insufficient to predict bone fracture because of heterogeneous properties and hierarchy structure of human cortical bone. So, a stress intensity factor related to extrinsic toughening mechanism, is also used to quantify the fracture resistance of human cortical bone. However, the understanding of the effect of micro-morphology of osteonal structure on fracture toughness of human cortical bone is still not fully established. The experimental analysis is not suitable for this investigation because of the difficulty of recording a crack path at micro-level and quantifying this effect without accounting for mechanical properties of cortical bone and its constituents. Therefore, a novel computational method is suggested and adopted to simulate crack propagation process in domains with a direct account for bone's micro-morphology. The research also covers quantification and modelling of soft tissues – muscles – playing (together with bones) important role in biomechanics of limbs. A high mismatch in mechanical properties of soft tissues both with the hard tissue and a prosthesis is a significant challenge. Numerical

simulations can provide solutions for this challenge and elucidate processes at the interface between the life tissues and engineering structures.

### References

[1] A. A. Abdel-Wahab, K. Alam, V. V. Silberschmidt, *Analysis of anisotropic viscoelastoplastic properties of cortical bone tissues*, J. Mech. Behav. Biomed. **4** (2013), 807–820.
[2] S. Li, E. Demirci, V. V. Silberschmidt, *Variability and anisotropy of mechanical behavior of cortical bone in tension and compression*, Mech. Mater. **21** (2012), 109–120.
[3] S. Li, A. A. Abdel-Wahab, V. V. Silberschmidt, *Analysis of fracture processes in cortical bone tissue*, Eng. Frac. Mech. **110** (2012), 448–458.
[4] S. Li, A. A. Abdel-Wahab, E. Demirci, V. V. Silberschmidt, *Penetration of cutting tool into cortical bone: Experimental and numerical investigation of anisotropic mechanical behavior*, J. Biomech. **47** (2014), 1117–1126.

## Experimental challenges for electro- and magnetoactive polymers

Paul Steinmann

In a nutshell, electro-active polymers (EAP) and magneto-active polymers (MAP) can be actuated with large deformations by either an electric field applied via flexible electrodes or a magnetic field applied contactless, respectively. The ability for extreme actuation makes EAP and MAP interesting candidates for soft actuators, e.g., in novel concepts for soft robotics. However, the fabrication, testing, and characterisation of this class of materials, needed as a necessary preliminary for their modelling and simulation, comes with a multitude of challenges.

Regarding EAPs, challenges reported on, e.g., in [1, 3, 4, 9, 10] are:

- the extreme compliance of the dielectric acrylic VHB polymer tape,
- the difficult specimen preparation and handling due to its stickyness,
- the necessity for pre-stretching the polymer tape in a controlled fashion,
- the application and influence of the flexible electrodes via conducting grease,
- the application and control of the electric field of up to 7 kV,
- the rate and temperature dependence of the polymer,
- among many others.

Regarding MAPs, challenges reported on, e.g., in [2, 5, 6, 7, 8] are:

- the agglomeration of the carbonyl iron filler particles during specimen fabrication,
- their sedimentation during the curing phase of the liquid silicone rubber matrix,
- the contact between the rotor surface and specimen during rotational rheometry,
- the application and control of the magnetic flux of up to 1 Tesla,
- the control of heat generation during testing,

- the rate and temperature dependence of the polymer,
- among many others.

The presentation gave a summarising, though brief, account on how to address these experimental challenges when investigating EAPs and MAPs.

## References


[1] Z. Liao, M. Hossain, X. Yao, M. Mehnert, P. Steinmann, *On thermo-viscoelastic experimental characterisation and numerical modelling of VHB polymer*, International Journal of Non-Linear Mechanics **118** (2020), 103263.

[2] J.P. Pelteret, P. Steinmann, *Magneto-Active Polymers: Fabrication, characterisation, modelling and simulation at the micro- and macro-scale*, De Gruyter (2019), ISBN 978-3-11-041951-1.

[3] M. Mehnert, M. Hossain, P. Steinmann, *Experimental and numerical investigations of the electro-viscoelastic behavior of VHB 4905*$^{\mathrm{TM}}$, European Journal of Mechanics / A Solids, **77** (2019), 103797.

[4] M. Mehnert, P. Steinmann, *On the influence of the compliant electrodes on the mechanical behavior of VHB 4905*, Computational Materials Science **160** (2019), 287–294.

[5] J.P. Pelteret, B. Walter, P. Steinmann, *Application of metaheuristic algorithms to the identification of nonlinear magneto-viscoelastic constitutive parameters*, Journal of Magnetism and Magnetic Materials **464** (2018), 116–131.

[6] B. Walter, J.P. Pelteret, J. Kaschta, D. Schubert, P. Steinmann, *On the wall slip phenomenon of elastomers in oscillatory shear measurements using parallel-plate rotational rheometry: I. Detecting wall slip*, Polymer Testing **61** (2017), 430–440.

[7] B. Walter, J.P. Pelteret, J. Kaschta, D. Schubert, P. Steinmann, *On the wall slip phenomenon of elastomers in oscillatory shear measurements using parallel-plate rotational rheometry: II. Influence of experimental conditions*, Polymer Testing **61** (2017), 455–463.

[8] B. Walter, J.P. Pelteret, J. Kaschta, D. Schubert, P. Steinmann, *Preparation of magnetorheological elastomers and their slip-free characterization by means of parallel-plate rotational rheometry*, Smart Materials and Structures **26** (2017), 085004.

[9] M. Hossain, D.K. Vu, P. Steinmann, *A comprehensive characterization of the electromechanically coupled properties of VHB 4910 polymer*, Archive of Applied Mechanics **85** (2015), 523–537.

[10] M. Hossain, D.K. Vu, P. Steinmann, *Experimental study and numerical modelling of VHB 4910 polymer*, Computational Materials Science **59** (2012), 65–74.


## GENERIC-based formulation of coarse-grained dislocation dynamics, transport and kinetics


Bob Svendsen

(joint work with Markus Hütter)


Collective dislocation behavior in metallic systems is highly dissipative in nature and results in the formation and evolution of a wide variety of microstructures. Discrete modeling approaches for this at the mesoscopic level include for example kinetic Monte Carlo or line dislocation dynamics (e.g., [1]). Related continuum modeling approaches are often based on direct averaging methods and phenomenological transport relations (e.g., [2, 3]). The inherent "slowness" of dislocation dynamics even on macroscopic timescales and concomitant lack of timescale separation motivates the application of more sophisticated coarse-graining methods. To

this end, following previous work (e.g., [4]), coarse-graining of dislocation dynamics is carried out in the current work in the context of non-equilibrium statistical thermodynamics with the help of projection-operator [5] and fluctuation-dissipation methods as well as the General Equation for Non-Equilibrium Reversible Irreversible Coupling [6]. Generalizing the straight dislocation treatment in [4], the current approach is based on the general elastic interaction energy functional for curved dislocation networks from dislocation field theory [7]. In particular, this formulation results in coarse-grained continuum balance, transport, and thermodynamic flux-force, relations depending on the underlying discrete energetics and dynamics. Although exact, the resulting functional relations are not computable. Analogous to the case of density functional theory, approximations and simplifications such as the local density approximation [8], or discretization in the sense of line dislocation dynamics [9], are necessary to this end and investigated here.

### References


[1] V. V. Bulatov, W. Cai, *Computer Simulation of Dislocations*, Oxford 2006.

[2] J. Deng, A. El-Azab, *Temporal statistics and coarse graining of dislocation ensembles*, Philosophical Magazine **90** (2010), 3651–3678.

[3] Y. S. Chen, W. Choi, S. Papanikolaou, M. Bierbaum, J. P. Sethna, *Scaling theory of continuum dislocation dynamics in three dimensions: Self-organized fractal pattern formation*, International Journal of Plasticity **46** (2013), 94–129.

[4] M. Kooiman, M. Hütter, M.G.D. Geers, *Effective mobility of dislocations from systematic coarse-graining*, Journal of Statistical Physics **10** (2015), PO6005.

[5] H. Grabert, *Projection Operator Techniques in Non-Equilibrium Statistical Mechanics*, Springer, 1982.

[6] H. C. Öttinger, *Beyond Equilibrium Thermodynamics*, Wiley Interscience, 2005.

[7] R. de Wit', *The continuum theory of stationary dislocations*, Solid State Physics **10**(C) (1960), 249–292.

[8] M. Zaiser, *Local density approximation for the energy functional of three-dimensional dislocation systems*, Physical Review B **92**(17) (2015), 174120.

[9] W. Cai, A. Arsenlis, C. R. Weinberger, V. V. Bulatov, *A non-singular continuum theory of dislocations*, Journal of the Mechanics and Physics of Solids **54**(3) (2006), 561–587.


## Temperature-dependent Mechanical Parameters: A Mechanical Motivation for studying Nonlocal, Parabolic PDEs


David Torkington

(joint work with Heiko Gimperlein, Andrew A. Lacey)


If a material is extremely energetic – that is, it possesses a large amount of stored chemical energy – then improper handling poses a serious safety concern, as even a mild deformation of the material could lead to heat build-up (through internal mechanical dissipation) that exceeds the energetic material's low activation energy. It is well attested by experiment that macroscopic mechanical parameters, such as viscosity and elastic modulus, vary with temperature. Hence, any heat build-up will affect the energetic material's mechanical response, in turn affecting the rate of any additional heat build-up due to mechanical dissipation. As such, due to the

extreme sensitivity of energetic materials, it is vital to account for the temperature dependence of the mechanical parameters.

Herein, a model to describe the heat evolution within a sheared one-dimensional material body with temperature-dependent mechanical parameters produces nonlocal, parabolic partial differential equations, thereby motivating both the analytical and numerical study of these equations. Analogous equations, but derived in different contexts, have been examined in [1] and [2], for example.

A one-dimensional material is considered, parametrised by the Eulerian ordinate $x \in [0,1]$. The material undergoes quasi-static simple shear (with *no* compression mode) in the $y$ direction, in the absence of body forces. We denote by $v(x,t)$ the material's pointwise velocity in the $y$ direction; by $\tau(x,t)$ the local shear stress experienced by the material; and by $\rho$, $c$ and $k$, the material's mass density, specific heat capacity, and thermal conductivity respectively, each taken to be constant in spacetime. The lateral velocity in the $y$ direction is specified at each of the boundary points: $v(0,t) \equiv 0$ and $v(1,t) = V(t)$, for $V(t)$ given.

The material must satisfy the local balances laws for momentum and energy:

$$\rho v_t = \tau_x, \text{ and} \tag{1}$$

$$\rho c T_t - k T_{xx} = \tau v_x. \tag{2}$$

The quantity $\tau v_x$ in the energy equation is the local heat released due to mechanical dissipation (per unit time). Since the material is sheared quasi-statically, equation (1) reduces to $\tau_x \approx 0 \Leftrightarrow \tau \approx \tau(t)$. The final expression will be taken to be an exact equality, serving to decouple (1) and (2).

Indeed, for example, considering an incompressible, thermo-viscous material described by the constitutive equation

$$\tau = \mu(T) v_x \tag{3}$$

(the pressure field can be neglected in this one-dimensional setting), where importantly, the (dynamic) viscosity $\mu = \mu(T)$ depends on the local temperature $T = T(x,t)$, we can obtain

$$v_x = \frac{\tau(t)}{\mu(T)} \implies V(t) - 0 = \int_0^1 v_x \, \mathrm{d}x = \tau(t) \int_0^1 \frac{1}{\mu(T)} \, \mathrm{d}x \,,$$

since $\tau$ is independent of space $x$ due to the quasi-static approximation. Hence, setting $\phi(T) := 1/\mu(T)$ and using (3), the local heat released due to mechanical dissipation (per unit time) within the thermo-viscous material is given by

$$\tau v_x = \frac{\tau^2(t)}{\mu(T)} \equiv \phi(T)\tau^2(t) = \frac{\phi(T) V^2(t)}{\left( \int_0^1 \phi(T) \, \mathrm{d}x \right)^2}, \tag{4}$$

yielding the following nonlocal, parabolic partial differential equation for the heat evolution:

$$\rho c T_t - k T_{xx} = \frac{\phi(T) V^2(t)}{\left( \int_0^1 \phi(T) \, \mathrm{d}x \right)^2}. \tag{5}$$

Similarly, considering an incompressible, Maxwellian-thermo-viscoelastic material (again the pressure field is not needed in this one-dimensional setting) described by the constitutive equation

$$\tau + \frac{\mu(T)}{G(T)}\dot{\tau} = \mu(T)v_x, \tag{6}$$

where the dynamic viscosity $\mu = \mu(T)$ and the shear elastic modulus $G = G(T)$ each depend on the local temperature $T(x,t)$. Still with $\phi(T) := 1/\mu(T)$ and setting $W(T) := 1/E(T)$, then, similar to before, we can obtain

$$V(t) - 0 = \int_0^1 v_x \,\mathrm{d}x = \tau(t)\int_0^1 \phi(T)\,\mathrm{d}x + \dot{\tau}(t)\int_0^1 W(T)\,\mathrm{d}x,$$

yielding the following ordinary differential equation for $\tau = \tau(t)$:

$$\dot{\tau}(t) + \frac{\int_0^1 \phi(T)\,\mathrm{d}x}{\int_0^1 W(T)\,\mathrm{d}x}\tau(t) = \frac{V(t)}{\int_0^1 W(T)\,\mathrm{d}x}. \tag{7}$$

For ease of notation, setting $\overline{f}(t) := \int_0^1 f(T)\mathrm{d}x$ for any temperature-dependent function $f(T)$, and imposing the stress-free initial condition $\tau(0) = 0$, (7) has solution formula

$$\tau(t) = \int_0^t \frac{V(t'')}{\overline{W}(t'')} \exp\left(-\int_{t''}^t \frac{\overline{\phi}(t')}{\overline{W}(t')}\,\mathrm{d}t'\right)\mathrm{d}t''. \tag{8}$$

As well as being nonlocal in space, through the terms $\overline{\phi}(t)$ and $\overline{W}(t)$, this expression exemplifies the memory property of the thermo-viscoelastic material, through the integration in time. This expression is too cumbersome for direct use as a source term in a nonlocal, parabolic partial differential equation, and so instead we take the elastic portion of the Maxwellian material to be asymptotically rigid, in the sense that there exist $0 < \varepsilon \ll 1$ and $r(T)$ such that

$$W(T) \equiv \frac{1}{G(T)} = \varepsilon r(T), \tag{9}$$

where the function $r(T)$ is independent of $\varepsilon$. The viscosity $\mu(T)$ is also taken to be independent of $\varepsilon$. We then expand the solution (8) as an asymptotic series in the small parameter $\varepsilon$, making the previously unwieldy nonlocal, parabolic partial differential equation more amenable to numerical analysis. This expansion must be done with care, due to the appearance of terms in $1/\varepsilon$, but we have succeeded in determining the zeroth- and first-order modes analytically.

Now that such nonlocal, parabolic partial differential equations have been motivated, we are investigating their well-posedness, as well as developing schemes to solve them numerically, both in the one-dimensional setting and in higher dimensions, after first generalising the equations to higher dimensions in the natural way. On this note, we are hoping to derive these higher-dimensional counterparts from first principles, rather than simply performing this generalisation step, but this requires more work than the one-dimensional case presented herein.

References

[1] N. Kavallaris, A. Lacey, C. Nikolopoulos, C. Voong, *Behaviour of a non-local equation modelling linear friction welding*, IMA Jl. Appl. Maths. **72** (2007), 597–616.

[2] H. Gimperlein, J. Stocek, *Space-time adaptive finite elements for nonlocal parabolic variational inequalities*, Computer Methods in Applied Mechanics and Engineering **352** (2019), 137–171.

## Application of crystal plasticity to nickel-based honeycomb structures under rubbing loading

Ewald Werner

(joint work with Tim Fischer, Sonan Ulan kyzy, Oliver Munz)

Sealing systems play a key role in the efficiency of gas turbine engines. The purpose of the sealing system is to keep the gap between the rotating and the stationary components as small as possible. This ensures a low leakage mass flow, thereby maintaining the pressure difference between the turbine stages resulting in a high efficiency and consequently a reduction in fuel consumption. However, due to the small gap widths, a contact between the components is much more likely. This procces is called rubbing. As stationary component of the sealing system, the honeycomb structures' role is to prevent catastrophic failure of the rotating component. During contact the honeycomb structure can also be critically damaged. Figure 1 illustrates the cross section of the honeycomb structure including the potential rubbing surface. Typical types of damage of the honeycomb structure are large and localised deformation, overheating, and crack initiation (mainly at the edges of the rubbing patch). The crack can subsequently cause large honeycomb structure parts to break out, thus compromising the functionality of the sealing system. Polycrystalline nickel-based superalloys are usually used as honeycomb structure material. Extreme thermo-mechanical loads are generated during rubbing, making the material properties of central importance. A variety of factors influence rubbing. Since most of these effects can only be determined to a limited degree with time-consuming and cost-intensive tests, it is aimed to capture the rubbing process in thermo-mechanical models taking into account the macro- and microstructure features of the honeycomb structure.

To achieve a detailed representation of the material response, the constitutive behaviour of the employed nickel-based superalloys Hastelloy X and Haynes 214 is modelled with a crystal plasticity approach, utilising a finite element framework. The material model is based on the multi-physics software tool DAMASK (developed at the Max-Planck-Institut für Eisenforschung, Düsseldorf) [1]. Using the crystal plasticity approach, it is assumed that plastic flow is mainly achieved by dislocation glide in slip systems. This allows to model effects influenced by individual grains and their respective orientation. The material model is designed for a wide range of temperatures and strain rates. In addition, isotropic thermal

expansion and the influence of the grain size are taken into account. As an introduction into the application of crystal plasticity, reference [1] is recommended. Further insights into the material model can be found in [2, 3, 4].
For an efficient rubbing simulation, the structural domain is restricted to the unit cell of the honeycomb structure (highlighted by the dashed box in Fig. 1) and periodic displacement boundary conditions (BCs) are applied to the outer faces of the cell. In addition, the bottom surface is fixed in $z$-direction. The thermomechanical loads acting on the rubbing surface are derived from experiments on a test rig [5]. A homogeneous temperature distribution is assumed at the beginning of the simulation. To further improve the efficiency of the rubbing simulation, the honeycomb structure is seperated into a core and an outer part (see Fig. 2). This modelling strategy is known as embedded cell approach [6, 7]. A similar approach was used in the past for fretting simulation [8, 9]. While the core part is provided with the crystal plasticity model, an isotropic plasticity model is assigned to the outer part. It is worth mentioning, that the wall thickness of the honeycomb structure is a few micrometers. Hence, the macroscopic scale of the honeycomb structure is of the same magnitude as the characteristic length of the microstructure of the material.
For the simulative study the mean grain size of the honeycomb structure is varied between $50 - 174\,\mu$m. In addition to the grain size, the influence of the grain orientation is investigated. A distinction is made between three different types of crystallographic grain orientation: (i) no texture (grain orientation is random), (ii) [111]-texture ([111] || $z$-axis), and (iii) [001]-texture ([001] || $z$-axis). The results of the study reveal that the macroscopic load of the honeycomb structure can be reduced by increasing the mean grain size. This can be attributed to the implemented grain size effect and the associated lower flow stress of the material. Moreover, a larger grain size leads to a greater spread of the loads for different random grain orientations. Similar to the grain size study, an effect of the grain

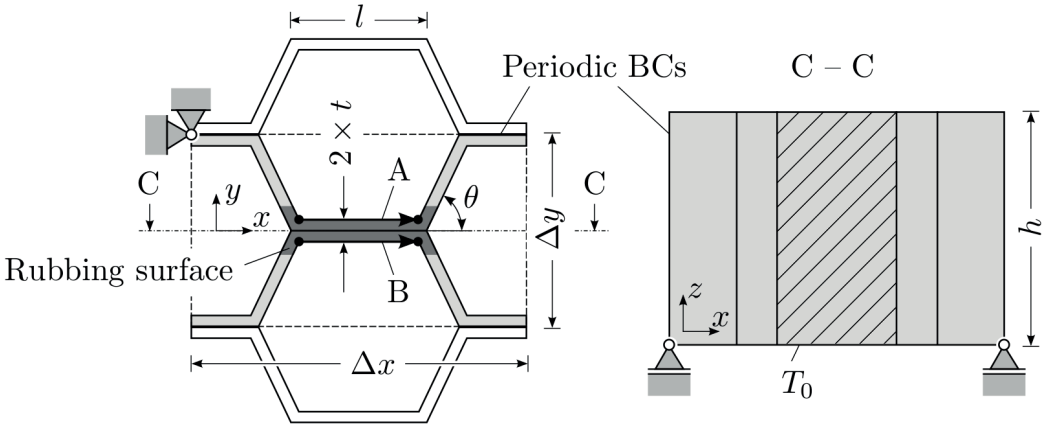


FIGURE 1. Geometry and boundary conditions (BCs) of the honeycomb structure for the rubbing simulation.

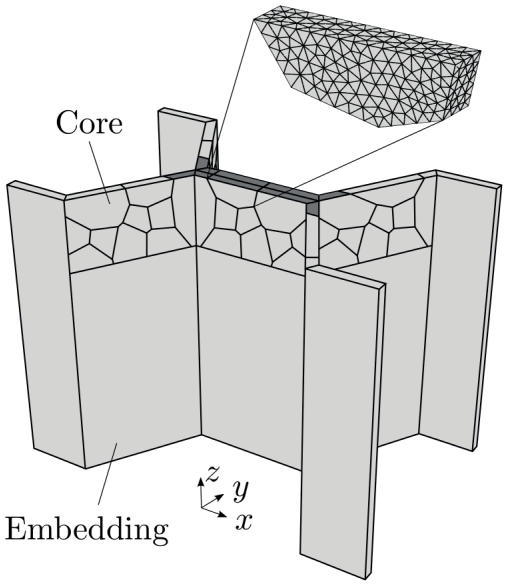


FIGURE 2. Embedded cell approach of the honeycomb structure consisting of a core part with a fully resolved microstructure embedded in a macroscopic outer part.

orientation is clearly observable. For the [001]-texture the macroscopic loads of both alloys are least pronounced. Finally, the studies show that the macroscopic load and the surface deformation occurring during rubbing are much greater for Haynes 214 than for Hastelloy X.

*Acknowledgment.* This work has been conducted in the context of the research project WE 2351/14-1, funded by the DFG (*Deutsche Forschungsgemeinschaft*).

## REFERENCES

[1] F. Roters, M. Diehl, P. Shanthraj, P. Eisenlohr, C. Reuber, S.L. Wong, T. Maiti, D. Ma, N. Jia, P.J.J. Kok, N. Fujita, A. Ebrahimi, T. Hochrainer, N. Grilli, K.G.F. Janssens, M. Stricker, D. Weygand, F. Meier, E. Werner, H.-O. Fabritius, S. Nikolov, M. Friak and D. Raabe, *DAMASK – The Düsseldorf Advanced Material Simulation Kit for modeling multi-physics crystal plasticity, thermal, and damage phenomena from the single crystal up to the component scale*, Computational Materials Science **158** (2019), 420–478.

[2] F. Meier, C. Schwarz, E. Werner, *Crystal-plasticity based thermo-mechanical modeling of Al-components in integrated circuits*, Computational Materials Science **94** (2014), 122–131.

[3] T. Fischer, E. Werner, S. Ulan kyzy, O. Munz, *Crystal plasticity modeling of polycrystalline Ni-base superalloy honeycombs under combined thermo-mechanical loading*, Continuum Mechanics and Thermodynamics **31** (2019), 703–713.

[4] T. Fischer, S. Ulan kyzy, O. Munz, E. Werner, *Microstructure-based modelling of rubbing in polycrystalline honeycomb structures*, Continuum Mechanics and Thermodynamics (2019), in print.

[5] O. Munz, T. Pychynski, C. Schwitzke, H. J. Bauer, *Continued experimental study on the friction contact between a labyrinth seal fin and a honeycomb stator: Slanted position*, Aerospace **5**(3) (2018), 82.

[6] E. Werner, R. Wesenjak, A. Fillafer, F. Meier, C. Krempaszky, *Microstructure-based modelling of multiphase materials and complex structures*, Continuum Mechanics and Thermodynamics **28** (2016), 1325–1346.
[7] H. J. Böhm, *A short introduction to basic aspects of continuum micromechanics*, ILSB Report, Vienna University of Technology **206** (1998).
[8] M. Zhang, D. L. McDowell, R. W. Neu, *Microstructure sensitivity of fretting fatigue based on computational crystal plasticity*, Tribology International **42** (2009), 1286–1296.
[9] M. Zhang, R. W. Neu, D. L. McDowell, *Microstructure-sensitive modeling: Application to fretting contacts*, International Journal of Fatigue **31** (2009), 1397–1406.

## Stress-free configurations in martensites and nematic liquid crystal elastomers

Barbara Zwicknagl
(joint work with P. Cesana, S. Conti, F. Della Porta, M. Klar, A. Rüland, C. Zillinger)

Shape memory alloys are special materials that undergo a martensitic phase transformation, i.e., a diffusionless, solid-to-solid phase transition of first order. The formation of microstructures in such materials is often modelled variationally in terms of the phenomenological theory of martensite [1] based on the geometrically nonlinear theory of elasticity.

Of recent interest are materials for which the high-temperature austenite and the low-temperature martensite phase are exceptionally compatible in the sense that exact interfaces without complicated microstructures are possible (see e.g. [2] and the references therein). Building on [3], we focus on highly compatible planar materials for which piecewise affine stress-free nuclei are possible. Mathematically, this corresponds to deformations $u : \mathbb{R}^2 \to \mathbb{R}^2$ which satisfy

$$\nabla u \in \begin{cases} SO(2) & \text{a.e. in } \Omega \\ \bigcup_{P\in\mathcal{P}} SO(2)P^TUP & \text{a.e. in } \mathbb{R}^2 \setminus \Omega, \end{cases} \tag{1}$$

where $\Omega \subset \mathbb{R}^2$ is the domain occupied by the martensitic nucleus, $U \in \mathbb{R}^{2\times 2}$ is a positive definite matrix that denotes a transformation matrix from austenite to one variant of martensite, and $\mathcal{P} \subset O(2)$ is the point group of the underlying austenite lattice. The SO(2)-invariance corresponds to the assumption of frame indifference.

Using the rotated $n$-gon construction from [4, 5], we identify crystallographic parameters for which piecewise affine solutions $u$ to (1) exist for a polygonal annular domain $\Omega$. This includes in particular certain cubic-to-oblique (for $n = 4$) and hexagonal-to-oblique (for $n = 3$) phase transitions [3].

These results can be also generalized and related to different phase transformations, see [6]. In particular, iterating such constructions in a self-similar way, one obtains (stressed) microstructures that are closely related to some experimentally observed tripole-star patterns (see [6] and the references given there). Furthermore, in the limit $n \to \infty$, the differential inclusion problem is related to models for nematic liquid crystal elastomers from [7, 8], see [6].

## References


[1] J.M. Ball and R.D. James. *Fine phase mixtures as minimizers of energy*, Arch. Rat. Mech. Anal. **100** (1987), 13–52.

[2] R.D. James. *Materials from mathematics*, Bull. Amer. Math. Soc. **56** (2019), 1–28.

[3] S. Conti, M. Klar and B. Zwicknagl. *Piecewise affine stress-free martensitic inclusions in planar nonlinear elasticity*, Proc. R. Soc. A **473** (2017), 20170235.

[4] S. Conti. *Quasiconvex functions incorporating volumetric constraints are rank-one convex*. J. math. pures appl. **90**(1) (2008), 15–30.

[5] W. Pompe. *Explicit construction of piecewise affine mappings with constraints*. Bull. Pol. Acad. Sc. Math., **58**(3) (2010), 209–220.

[6] P. Cesana, F. Della Porta, A. Rüland, C. Zillinger and B. Zwicknagl. *Exact Constructions in the (Non-linear) Planar Theory of Elasticity: From Elastic Crystals to Nematic Elastomers*. Arch. Rat. Mech. Anal., online first (2020). https://doi.org/10.1007/s00205-020-01511-9

[7] P. Bladon, M. Warner, and E.M. Terentjev. *Orientational order in strained nematic networks*. Macromolecules **27** (1994), 7067–7075.

[8] V. Agostiniani, G. Dal Maso and A. DeSimone. *Attainment results for nematic elastomers*. Proc. R. Soc. Edin. A: Math. **145**(4) (2015), 669–701.


*Reporter: Ewald A. Werner*

# Participants

**Dr. B. Emek Abali**
Institut für Mechanik
FG Kontinuumsmechanik und Materialtheorie
Technische Universität Berlin
Sekr. MS 2
Einsteinufer 5
10587 Berlin
GERMANY

**Prof. Dr.-Ing.habil.Dr.h.c.mult. Holm Altenbach**
Fakultät für Maschinenbau
Otto-von-Guericke-Universität Magdeburg
Universitätsplatz 2
39106 Magdeburg
GERMANY

**Dr.-Ing. Marcus Aßmus**
Institut für Mechanik
Otto-von-Guericke-Universität Magdeburg
Universitätsplatz 2
39106 Magdeburg
GERMANY

**Prof. Dr. Albrecht Bertram**
Institut für Mechanik
FG Kontinuumsmechanik und Materialtheorie
Technische Universität Berlin
Einsteinufer 5
10587 Berlin
GERMANY

**Prof. Dr. Irene J. Beyerlein**
Department of Mechanical Engineering
Materials Department
University of California, Santa Barbara
Santa Barbara, CA 93106-5070
UNITED STATES

**Dr. Martin Diehl**
Max-Planck-Institut für Eisenforschung GmbH
Max-Planck-Strasse 1
40237 Düsseldorf
GERMANY

**Prof. Dr. Anter A. El-Azab**
School of Materials Engineering and School
of Nuclear Engineering, ARMS 2215
Purdue University
701 West Stadium Avenue
West Lafayette, IN 47907-2045
UNITED STATES

**Prof. Dr. Samuel Forest**
Centre des Matériaux
MINES Paristech
CNRS UMR 7633
BP 87
91003 Évry Cedex
FRANCE

**Prof. Dr. Gilles A. Francfort**
LAGA UMR 7539
Institut Galilee
Université Paris XIII
99, Avenue Jean-Baptiste Clément
93430 Villetaneuse Cedex
FRANCE

**Prof. Dr. Thomas Hochrainer**
Institut für Festigkeitslehre
Technische Universität Graz
Kopernikusgasse 24/I
8010 Graz
AUSTRIA

**Prof. Dr.-Ing. Markus Kästner**
Institut für Festkörpermechanik
Fakultät Maschinenwesen
Technische Universität Dresden
01062 Dresden
GERMANY

**Prof. Dipl.-Ing. Björn Kiefer**
Institut für Mechanik und Fluiddynamik
Technische Universität Bergakademie Freiberg
Akademiestrasse 6
09599 Freiberg
GERMANY

**Prof. Dr.-Ing. Reinhold Kienzler**
FB 4 / FG 15 / IW 3
Universität Bremen
Postfach 330440
28334 Bremen
GERMANY

**Dr. Sven Klinkel**
Fakultät für Bauingenieurwesen
RWTH Aachen
Mies-van-der-Rohe-Strasse 1
52074 Aachen
GERMANY

**Prof. Dr. Dorothee Knees**
FB 10 - Mathematik und Naturwissenschaften
Institut für Mathematik
Universität Kassel
Heinrich-Plett-Strasse 40
34132 Kassel
GERMANY

**PD Dr.-Ing. Christian Krempaszky**
Lehrstuhl für Werkstoffkunde und Werkstoffmechanik
Technische Universität München
Boltzmannstrasse 15
85748 Garching bei München
GERMANY

**Prof. Dr. Khanh Chau Le**
Lehrstuhl für Allgemeine Mechanik
Fakultät für Bauingenieurwesen
Ruhr-Universität Bochum
Universitätsstrasse 150
44801 Bochum
GERMANY

**Prof. Dr. Wing Kam Liu**
Department of Mechanical Engineering
Robert R. McCornick School of Engineering
Northwestern University
2145 Sheridan Road
Evanston, IL 60208-3199
UNITED STATES

**Prof. Dr. Rolf Mahnken**
Lehrstuhl für Technische Mechanik
Universität Paderborn
Warburger Strasse 100
33098 Paderborn
GERMANY

**Michael Meyer-Coors**
FB 4 / FG 15 / IW 3
Universität Bremen
Postfach 330440
28334 Bremen
GERMANY

**Prof. Dr. Alexander Mielke**
Weierstraß-Institut für Angewandte Analysis und Stochastik
Mohrenstrasse 39
10117 Berlin
GERMANY

**Prof. Dr. Stefan Müller**
Hausdorff Center for Mathematics
Institute for Applied Mathematics
Endenicher Allee 60
53115 Bonn
GERMANY

**Prof. Dr. Wolfgang Helmut Müller**
Institut für Mechanik, Sekr. MS 2
FG Kontinuumsmechanik und Materialtheorie
Technische Universität Berlin
Einsteinufer 5
10587 Berlin
GERMANY

**Prof. Dr. Eugen Rabkin**
Department of Materials Science and Engineering
TECHNION - Israel Institute of Technology
Haifa 3200003
ISRAEL

**Dr. Franz Roters**
Max-Planck-Institut für Eisenforschung GmbH
Max-Planck-Strasse 1
40237 Düsseldorf
GERMANY

**Prof. Dr. Anja Schlömerkemper**
Institut für Mathematik
Universität Würzburg
Emil-Fischer-Straße 40
97074 Würzburg
GERMANY

**Prof. Dr.-Ing. Jörg Schröder**
Institut für Mechanik
Abteilung Bauwissenschaften
Universität Duisburg-Essen
Universitätsstrasse 15
45141 Essen
GERMANY

**Prof. Dr. Vadim V. Silberschmidt**
The Wolfson School of Mechanical, Electrical
and Manufacturing Engineering
Loughborough University
Epinal Way
Loughborough, Leicestershire LE11 3TU
UNITED KINGDOM

**Prof. Dr. Paul Steinmann**
Lehrstuhl für Technische Mechanik
FAU Erlangen-Nürnberg
Egerlandstrasse 5
91058 Erlangen
GERMANY

**Prof. Dr. Robert Svendsen**
Lehrstuhl für Werkstoffmechanik
RWTH Aachen
Schinkelstrasse 2
52062 Aachen
GERMANY

**David Torkington**
Department of Mathematics
Heriot-Watt University
Riccarton
Edinburgh EH14 4AS
UNITED KINGDOM

**Prof. Dr. Ewald A. Werner**
Lehrstuhl für Werkstoffkunde und Werkstoffmechanik
Technische Universität München
Boltzmannstrasse 15
85748 Garching bei München
GERMANY

**Prof. Dr.-Ing. Bernd W. Zastrau**
Fakultät Bauingenieurwesen
Institut für Mechanik und Flächentragwerke
Technische Universität Dresden
August-Bebel-Straße 30
01219 Dresden
GERMANY

**Prof. Dr. Barbara Zwicknagl**
Institut für Mathematik
Humboldt-Universität zu Berlin
Rudower Chaussee 25
12489 Berlin
GERMANY